

Predictability and semiclassical approximation at the onset of black hole formation

Sukanta Bose,^{*} Leonard Parker,[†] and Yoav Peleg[‡]

Department of Physics

University of Wisconsin-Milwaukee, P.O.Box 413

Milwaukee, Wisconsin 53201, USA

Abstract

We combine analytical and numerical techniques to study the collapse of conformally coupled massless scalar fields in semiclassical 2D dilaton gravity, with emphasis on solutions just below criticality when a black hole almost forms. We study classical information and quantum correlations. We show explicitly how recovery of information encoded in the classical initial data from the outgoing classical radiation becomes more difficult as criticality is approached. The outgoing quantum radiation consists of a positive-energy flux, which is essentially the standard Hawking radiation, followed by a negative-energy flux which ensures energy conservation and guarantees unitary evolution through strong correlations with the positive-energy Hawking radiation. As one reaches the critical solution there is a breakdown of unitarity. We show that this breakdown of predictability is intimately related to a breakdown of the semiclassical approximation.

PACS numbers: 04.60.Kz, 04.70.Dy

^{*}Electronic address: *bose@csd.uwm.edu*

[†]Electronic address: *leonard@cosmos.phys.uwm.edu*

[‡]Electronic address: *yoav@csd.uwm.edu*

I. INTRODUCTION

Quantum radiation from black holes [1] is necessary in order to maintain the consistency of the second law of thermodynamics with the existence of black holes [2]. On the other hand, evaporation of the black hole reveals one of the most fundamental problems in theoretical physics; the question of unitary evolution of the Universe. Does evolution from an initial pure state take place non-unitarily to a final mixed state [3], or unitarily to a final pure state [4] ? One of the major obstacles to a better understanding of the Hawking effect is the complexity of four-dimensional (4D) semi-classical gravity [5]. Simplified models which may give insight into the possible answers are two-dimensional (2D) dilaton quantum gravity theories [6]. The dilaton field, viewed as part of the geometrical structure restores dynamics in 2D analogous to that of spherically symmetric 4D Einstein gravity. We consider the formation and evaporation of a 2D black hole by the collapse of massless matter scalar fields. The evaporation of the black hole via production of quanta of the matter fields can be fully traced in the 2D semiclassical theory, including the back-reaction of the evaporation on the geometry [7–11].

If the energy and energy density of the infalling matter are sufficiently large, then the incoming matter forms a black hole. Otherwise, the original incoming matter escapes to infinity and no black hole is formed. In this latter case the evolution is unitary and no information is lost. These unitary solutions of the semiclassical theory are called subcritical solutions [12–15]. The study of subcritical solutions just below the critical threshold in which a black hole is formed may help us to understand the process of semiclassical black hole formation and its influence on information. Moreover, the interesting results obtained in classical gravity concerning critical behavior at the onset of classical black hole formation [16] make it important to examine this critical behavior in the context of semiclassical physics. In the critical regime of the 4D Schwarzschild black hole, the black hole mass approaches zero and the curvature near the horizon becomes large, so semiclassical effects must be considered. Since the 4D semiclassical theory is quite complicated, insight may be gained by considering a 2D theory that shares many of its dynamical features, namely, 2D dilaton gravity [6]. The 2D dilaton models can be derived from 4D almost extremal dilatonic black holes [17] using the Kaluza-Klein reduction [18].

Although the general properties of the 2D subcritical solutions, namely that they are stable and unitary, have been known for sometime [12–14], investigation of the explicit evolution reveals some new features of physical importance [15]. In Ref. [15] we studied the evolution of the subcritical solutions with infalling matter in the form of shock-waves. In this work we extend our study to include the behavior of subcritical solutions for general smooth initial data, with emphasis on the near-critical solutions.

In Sec. II we present our model of 2D semiclassical dilaton gravity as an initial value problem. We also derive the general equations to be integrated numerically for arbitrary initial data. In Sec. III we give examples involving smooth infalling matter. The previous shock-wave results [15] appear as a limiting case of these examples.

In Sec. IV we address the question of information. The information that may be lost in the process of black hole evaporation is related to the correlations between the outside world and the interior of the black hole. Two types of information are involved: (i) “Classical information”, carried by the classical matter that forms the black hole, and (ii) “Quantum

information”, encoded in quantum correlations between outgoing and incoming pairs of particles created by the collapse geometry. A quantity that plays an important role in understanding the structure of the subcritical solutions is the outgoing radiation reaching future asymptotic null infinity, \mathfrak{S}_R^+ . In previous work [15] an explicit form of that radiation was found for the first time in semiclassical gravity. This outgoing radiation is intimately related to the question of information. In principle, for the subcritical solutions one should be able to recover the complete information given by the initial data from that outgoing radiation. We show how in the subcritical solutions, classical and quantum information is encoded in the outgoing radiation reaching asymptotic future null infinity.

In Sec. V we consider the subcritical solutions just below criticality. We show that as in the classical case, also in the semiclassical case solution space can be divided continuously into two regions, i.e., there exist continuously varying parameters, p_i , in solution space, such that for $p_i < p_i^*$ the evolved scalar field will not form a black hole (the subcritical solutions), while for $p_i > p_i^*$ a black hole will be formed (the supercritical solutions). We show that as the critical solution is approached ($p_i \rightarrow p_i^*$) the outgoing energy flux diverges and the fluctuations in the outgoing energy density become very large, implying a break down of the semiclassical approximation at criticality.

In Sec. VI we show that near criticality the density of information encoded in the outgoing radiation reaching \mathfrak{S}_R^+ becomes very large and diverges at criticality. This divergence results in an apparent breakdown of predictability that coincide with the breakdown of the semiclassical approximation. We present our conclusions in Sec. VII.

II. THE MODEL

A. 1-loop effective action

Recently we have proposed a modified theory of 2D semiclassical dilaton gravity [10]. The effective action of the modified theory is

$$S_{\text{eff}} = S_{CGHS} + N S_{PL} + S_{\text{corr}}, \quad (1)$$

where S_{CGHS} is the Callan-Giddings-Harvey-Strominger (CGHS) classical action [19],

$$S_{CGHS} = \frac{1}{2\pi} \int d^2x \sqrt{-g} \left[e^{-2\phi} \left(R^{(2)} + 4(\nabla\phi)^2 + 4\lambda^2 \right) - \frac{1}{2} \sum_{i=1}^N (\nabla f_i)^2 \right], \quad (2)$$

S_{PL} is the Polyakov-Liouville action [20] that incorporates the 1-loop corrections corresponding to the trace anomaly of the stress energy momentum tensor of each of the N quantum matter fields,

$$S_{PL} = -\frac{\hbar}{96\pi} \int d^2x \sqrt{-g(x)} \int d^2x' \sqrt{-g(x')} R^{(2)}(x) G(x, x') R^{(2)}(x'), \quad (3)$$

and

$$S_{\text{corr}} = \frac{N\hbar}{24\pi} \int d^2x \sqrt{-g} \left((\nabla\phi)^2 - \phi R^{(2)} \right) \quad (4)$$

is a local counter-term that we add in order to get an exactly solvable theory. In the above ϕ is the dilaton field, $R^{(2)}$ is the 2D Ricci scalar, λ is a positive constant, ∇ is the covariant derivative, and $G(x, x')$ is an appropriate Green's function for ∇^2 . The N real value functions, $f_i(x)$, are the classical values of the massless scalar fields. One can regard each of the $f_i(x)$ as the expectation value of the quantum field operator, $\hat{f}_i(x)$, in an appropriate quasi classical coherent state, $|\alpha\rangle$ [21]. The effective action (1) describes the full quantum theory in the large N limit, in which case the fluctuations of ϕ and $g_{\mu\nu}$ can be neglected [12,10]. Recently Miković showed that one can derive the effective action of Eq. (1) from S_{CGHS} by fixing the diffeomorphism gauge, solving the constraints, and then quantizing the reduced system. After choosing an appropriate initial quantum state, one recovers the action (1) as a 1-loop effective action [22].

In null coordinates, z^\pm , and conformal gauge, $g_{++} = g_{--} = 0$, $g_{+-} = -(1/2)\exp(2\rho)$, the action (1) takes the form

$$S_{\text{eff}} = \frac{1}{\pi} \int dz^+ dz^- \left[(\partial_- Y) \partial_+ (X - \frac{\kappa}{2} Y) + (\partial_+ Y) \partial_- (X - \frac{\kappa}{2} Y) + \lambda^2 \exp(-2Y) + \frac{1}{2} \sum_{i=1}^N \partial_+ f_i \partial_+ f_i \right], \quad (5)$$

where $X \equiv \exp(-2\phi)$, $Y \equiv \phi - \rho$, and $\kappa = N\hbar/12$. In the large N limit we take \hbar to approach zero while keeping κ finite. The kinetic action density of the system described in Eq. (5) is a bilinear symmetric form $(\partial_+ \Theta) M(\phi) (\partial_- \Theta)$, where Θ is a vector comprised of the $(N+2)$ fields X, Y and the N matter fields, f_i , and $M(\phi)$ is an $(N+2) \times (N+2)$ symmetric matrix. One can verify that the determinant of M is proportional to $X^2 = \exp(-4\phi)$, and unlike in other models of modified dilaton gravity [7], here this determinant is non-vanishing for all real values of ϕ . The vanishing of the determinant at $X(x^+, x^-) = 0$ signals a singularity.

The equations of motion derived from varying the action (4) with respect to X, Y and f_i are

$$\partial_+ \partial_- X = -\lambda^2 \exp(-2Y), \quad (6)$$

$$\partial_+ \partial_- Y = 0, \quad (7)$$

$$\partial_+ \partial_- f_i = 0. \quad (8)$$

The constraints (from varying the action (1) with respect to $g_{\pm\pm}$) are

$$-\partial_\pm^2 X - 2\partial_\pm X \partial_\pm Y - T_{\pm\pm}^{cl} + \kappa \left[(\partial_\pm Y)^2 + \partial_\pm^2 Y + t_\pm(z^\pm) \right] = 0, \quad (9)$$

where after varying with respect to $g_{\mu\nu}$ ($\mu = \pm, \nu = \pm$) we set $g_{++} = g_{--} = 0$ to get (9). Here $T_{\pm\pm}^{cl} = (1/2) \sum_i (\partial_\pm f_i)^2$ is the classical contribution to the energy-momentum tensor of the N matter fields, and $t_\pm(z^\pm)$ are integration functions determined by the specific quantum state of the matter scalar fields. A conformal coordinate transformation of the form $z^+ \rightarrow y^+$ and $z^- \rightarrow y^-$, preserves the form of the metric, $g_{\pm\pm} = 0$ and $g_{+-} = -(1/2)\exp(2\bar{\rho})$, where the new conformal mode function is related to the old one by $\bar{\rho}(y^+, y^-) = \rho(z^+, z^-) + \ln \sqrt{dz^+/dy^+} + \ln \sqrt{dz^-/dy^-}$. The dilaton field is a scalar, and therefore the field Y transforms like $-\rho$. The general solution of Eq. (7) for Y is $Y(z^+, z^-) =$

$Y_+(z^+) + Y_-(z^-)$, and we can choose the coordinates $x^\pm = \int^{z^\pm} \exp[-2Y_\pm(\tilde{z}^\pm)] d\tilde{z}^\pm$, for which $Y(x^+, x^-) \equiv 0$. In the following we use these ‘‘Kruskal’’ coordinates, denoted by (x^+, x^-) , for which $\phi(x^+, x^-) = \rho(x^+, x^-)$. Henceforth, the indices \pm on tensors will refer to components in the Kruskal coordinates.

In the Kruskal gauge the general solutions to (6) and (8), subject to the constraints (9), are

$$\begin{aligned} X(x^+, x^-) = & -\lambda^2 x^+ x^- - \int^{x^+} dx_2^+ \int^{x_2^+} dx_1^+ [T_{++}^{cl}(x_1^+) - \kappa t_+(x_1^+)] \\ & - \int^{x^-} dx_2^- \int^{x_2^-} dx_1^- [T_{--}^{cl}(x_1^-) - \kappa t_-(x_1^-)] \end{aligned} \quad (10)$$

and

$$f_i(x^+, x^-) = f_i^+(x^-) + f_i^-(x^+). \quad (11)$$

B. The initial value problem

Consider first the linear dilaton (LD) solution which corresponds to $f_i(x^+, x^-) = 0$ and $t_\pm(x^\pm) = 0$ in (10), namely, the solution $X_{LD}(x^+, x^-) = -\lambda^2 x^+ x^-$. It is defined for $0 < x^+ < \infty$ and $-\infty < x^- < 0$. In the manifestly flat coordinates, $\sigma^\pm \equiv \tau \pm \sigma = \pm \lambda^{-1} \ln(\pm \lambda x^\pm)$, the LD solution corresponds to the flat metric, $ds^2 = -d\sigma^+ d\sigma^-$, and the dilaton field has the linear form, $\phi = -\lambda\sigma$. As shown in Fig. 1, the null curve $x^+ = 0$ defines left asymptotic past null infinity, \mathfrak{S}_L^- , the null curve $x^- = -\infty$ defines right asymptotic past infinity, \mathfrak{S}_R^- . The null curve $x^- = 0$ is left asymptotic future infinity, \mathfrak{S}_L^+ and $x^+ = +\infty$ is right asymptotic future infinity, \mathfrak{S}_R^+ . In general, the initial data on \mathfrak{S}_L^- and \mathfrak{S}_R^- determine completely the solution in the region $0 < x^+ < \infty$, $-\infty < x^- < 0$. Specifying these initial data is equivalent to giving $f_i^-(x^-)$, and $t_-(x^-)$ on \mathfrak{S}_L^- and $f_i^+(x^+)$ and $t_+(x^+)$ on \mathfrak{S}_R^- . Giving these functions, we integrate (10) to find the solution everywhere, however such a solution may not be physically acceptable in the whole space-time, since singularities may appear. One can say that our 1-loop effective theory is exactly solvable however there is one major difficulty with such an approach. Consider first the LD solution: while on \mathfrak{S}_R^- we have $\sigma \rightarrow \infty$ and $\exp(2\phi) = 0$, on \mathfrak{S}_L^- ($\sigma \rightarrow -\infty$) we have $\exp(2\phi) \rightarrow \infty$. From the action (2) we see that $\exp(2\phi)$ plays the role of the ‘‘coupling constant’’, and so the coupling *diverges* on \mathfrak{S}_L^\pm . One can split the space-time into a region of weak coupling and a region of strong coupling, see Fig. 1. Those two regions are divided by a curve, the ‘‘boundary curve’’ (specified below in more detail). In the strong coupling region we cannot trust the 1-loop effective theory, especially on \mathfrak{S}_L^\pm . Therefore giving the initial data on \mathfrak{S}_L^- is in general unphysical. One way to avoid this problem is to consider the solutions only in the weak coupling region and impose on a time-like curve boundary conditions that preserve unitarity and conserve energy. These criteria are satisfied by imposing reflecting boundary conditions on the boundary curve. Thus, the initial value problem that we define is the following: on \mathfrak{S}_R^- we give the initial data, $f_i^+(x^+)$ and $t_+(x^+)$, and on the boundary curve defined by $x^+ = x_B^+(x^-) \equiv p(x^-)$, we impose the reflecting boundary condition.

Before specifying the boundary condition we elaborate on the energy-momentum tensor. The c-number $T_{\mu\nu}^f$, which one gets after varying the effective action in (1) with respect to the metric $g^{\mu\nu}$, can be regarded as the expectation value of the quantum operator, $\hat{T}_{\mu\nu}^f$, in the quasi-classical coherent state, $|\alpha\rangle$, [21]. Namely,

$$T_{\mu\nu}^f \equiv \langle \alpha | \hat{T}_{\mu\nu}^f | \alpha \rangle = T_{\mu\nu}^{cl} + \langle T_{\mu\nu} \rangle ,$$

where in the expansion of $\langle \alpha | \hat{T}_{\mu\nu}^f | \alpha \rangle$ the first term, $T_{\mu\nu}^{cl}$, is of order \hbar^0 and is the classical part of the stress tensor, while the second term, $\langle T_{\mu\nu} \rangle$, is of order \hbar (or $N\hbar$ for N fields) and is the one-loop contribution. The one-loop contribution to the energy-momentum tensor is given by

$$\langle T_{z^\pm z^\pm} \rangle = \kappa [\partial_{z^\pm}^2 \rho - (\partial_{z^\pm} \rho)^2 - t_{z^\pm}(z^\pm)] \quad ; \quad \langle T_{z^+ z^-} \rangle = \kappa \partial_{z^+} \partial_{z^-} \rho , \quad (12)$$

in some general null coordinates (z^+, z^-) . Equation (12) follows by integrating $\nabla_\mu \langle T^{\mu\nu} \rangle = 0$ and using the trace anomaly [23] $\langle T_\mu^\mu \rangle = -\kappa R^{(2)}/2$ for the N massless matter fields \hat{f}_i [24], or equivalently by varying the Polyakov-Liouville action (3) with respect to the metric [20].

One can argue that operationally the split between the classical and quantum radiation is not well-defined when we consider a single (scalar) field. However, for N fields one could classically excite only some of the fields. Then the total radiation in the remaining fields is just the quantum part. To operationally distinguish among the N fields, one can, for example, add another quantum number to these scalar fields.

The reflecting boundary condition is [25,13,5,15]

$$T_{--}^f(x^-) = (p'(x^-))^2 T_{++}^f(x_B^+(x^-)) + \kappa (p'(x^-))^{1/2} \partial_-^2 (p'(x^-))^{-1/2} \quad (13)$$

where $' = \partial/\partial x^-$. The last expression on the right hand side (r.h.s.) of Eq. (13) is due to quantum particle creation from the boundary, which is effectively a moving mirror [5,25]. One can split the reflecting boundary condition (13) into its classical and 1-loop parts,

$$T_{--}^{cl}(x^-) = (p'(x^-))^2 T_{++}^{cl}(x_B^+(x^-)) \quad (14)$$

$$t_-(x^-) = (p'(x^-))^2 t_+(x_B^+(x^-)) + \frac{(p'(x^-))^{1/2} \partial_-^2 (p'(x^-))^{-1/2}}{1 + \kappa/(2X_B)} \quad (15)$$

If we take the fields f_i to satisfy Neumann or Dirichlet boundary conditions, then the classical reflecting boundary condition (14) is satisfied.

Next we consider the boundary curve. We would like it to separate the regions of weak coupling, $\exp(2\phi) < g_c^2$, and strong coupling, $\exp(2\phi) > g_c^2$, where g_c^2 is some parameter that specifies the value of the coupling below which the 1-loop effective theory is trustworthy. Since $X(x^+, x^-) = \exp(-2\phi)$, we can define the boundary curve to be the curve on which $X(x^+, x^-) = X_B \equiv g_c^{-2} = \text{const}$. The solution $X(x^+, x^-)$ should be determined by the initial data on \mathfrak{S}_R^- and by the boundary condition (13). The boundary curve, $X(x^+, x^-) = X_B$, depends on the solution $X(x^+, x^-)$. Thus, we get a highly non-linear problem, unlike the straightforward problem, with initial data given on \mathfrak{S}^- , having solutions (10) and (11). We next reduce this non-linear problem to solving a single ordinary differential equation.

C. The boundary equation as a second order ODE

The function $T_{++}^{cl}(x^+)$ can be viewed as the part of the initial data on \mathfrak{S}_R^- that describes the classical profile of the infalling matter. We take $T_{++}^{cl}(x^+)$ to be a general function of x^+ with compact support. On the other hand, $t_+(x^+)$ describes the quantum state on \mathfrak{S}_R^- . Since in this work we would like to study the Hawking effect, we take the quantum state to be such that on \mathfrak{S}_R^- we have no quantum radiation, (i.e., $\langle T_{vv} \rangle(v) = 0$, where v is the asymptotically flat null coordinate on \mathfrak{S}_R^- , $v = \lambda^{-1} \ln(\lambda x^+)$). Since in the asymptotically flat null coordinates the conformal mode, ρ , approaches zero on \mathfrak{S}_R^- , we get from (12) that in these coordinates $t_v(v) = 0$. To find the corresponding $t_+(x^+)$ in Kruskal coordinates, we use the tensor transformation of $\langle T_{z^\pm z^\pm} \rangle$ in Eq. (12) (under a conformal coordinate transformation) and get

$$t_+(x^+) = \left(\frac{\partial v}{\partial x^+} \right)^2 \left(t_v(v) - \frac{1}{2} D_v^S[x^+] \right) = \frac{1}{(2x^+)^2} , \quad (16)$$

where $D_y^S[z]$ is the Schwarz operator defined as

$$D_y^S[z] = (\partial_y^3 z) / (\partial_y z) - \frac{3}{2} (\partial_y^2 z / \partial_y z)^2 \quad (17)$$

and we use $t_v(v) = 0$. Eq. (15) then becomes

$$t_-(x^-) = \frac{1}{4} \left(\frac{p'(x^-)}{p(x^-)} \right)^2 + \frac{(p'(x^-))^{1/2} \partial_-^2 (p'(x^-))^{-1/2}}{1 + \kappa / (2X_B)} . \quad (18)$$

The second term on the r.h.s. of Eq. (18) is the result of particle creation from the dynamical boundary. Recall that in the 4D Hawking effect [1], the ‘‘boundary curve’’ is $r = 0$ (the fixed point of spherical symmetry). The curve $r = 0$ does not act as a moving mirror and there is no particle creation at $r = 0$. The creation of particles (i.e., the Hawking radiation) is due to the curvature of space-time near the horizon. Can we also eliminate the moving mirror effect in our 2D theory? We see from (18) that if $X_B \ll \kappa$, then the moving mirror term is negligible. This is consistent with the fact that $X = \exp(-2\phi)$ is indeed the 4D radial coordinate [18,26], and $X_B \rightarrow 0$ corresponds to $r \rightarrow 0$ in 4D. However, one should be careful when taking the limit $X_B \rightarrow 0$. It corresponds to the limit $g_c^2 \rightarrow \infty$, which defines the strong coupling region. The 1-loop effective theory (1) is trustworthy as long as $g_c^2 \hbar \ll \kappa \ll 1$. In this case (in the region of interest, i.e., $X(x^+, x^-) \geq X_B$) the quantum corrections for the dilaton-gravity part are negligible compare to the 1-loop corrections for the N scalar fields, which in turns are small compared to the classical contribution. Therefore, we need to satisfy both $g_c^2 \hbar \ll \kappa \ll 1$ and $X_B \ll \kappa$. With $X_B^{-1} = g_c^2$, we combine the conditions and get

$$\frac{1}{N} \ll X_B \ll N \hbar \ll 1. \quad (19)$$

One can always take the large N limit in such a way that (19) is satisfied and X_B is arbitrarily close to zero. In the following we take this large N limit. Eq. (18) then reduces to

$$t_-(x^-) = \frac{1}{4} \left(\frac{p'(x^-)}{p(x^-)} \right)^2. \quad (20)$$

One can write the general solution (10) in the form

$$X(x^+, x^-) = -\lambda x^+ (\lambda x^- + \lambda^{-1} P_+(x^+)) - \frac{\kappa}{4} \ln(\lambda x^+) + \frac{M(x^+)}{\lambda} + F(x^-), \quad (21)$$

where $M(x^+)$ and $P_+(x^+)$ are the mass and momentum of the infalling classical matter,

$$M(x^+) \equiv \lambda \int_0^{x^+} x_1^+ T_{++}^{cl}(x_1^+) dx_1^+ \quad , \quad P_+(x^+) \equiv \int_0^{x^+} T_{++}^{cl}(x_1^+) dx_1^+ \quad , \quad (22)$$

and

$$F(x^-) \equiv - \int^{x^-} dx_2^- \int^{x_2^-} dx_1^- [T_{--}^{cl}(x_1^-) - \kappa t_-(x_1^-)] \quad . \quad (23)$$

Here $F(x^-)$ is a function of x^- to be determined by the boundary conditions. Before we obtain the equation for the boundary curve, let us define the following dimensionless quantities:

$$z \equiv \lambda x^- \quad \text{and} \quad q(z) \equiv \lambda x_B^+(x^-(z)) = \lambda p(x^-(z)) \quad , \quad (24)$$

where $q(z)$ is a dimensionless function that specifies the location of the boundary curve. Using (9), (20), (21) and acting with $\partial^2/\partial z^2$ on the boundary equation $X(x_B^+, x^-) = X_B$, we get a second order ODE for $q(z)$

$$\left[z + P_q(q) + \frac{\kappa}{4q(z)} \right] \frac{d^2 q}{dz^2} + 2 \frac{dq}{dz} + 2 \left[T_{qq}^{cl}(q) - \frac{\kappa}{4q^2(z)} \right] \left(\frac{dq}{dz} \right)^2 = 0, \quad (25)$$

where

$$T_{qq}^{cl}(q) \equiv \lambda^2 T_{++}(x_B^+(x^-)) \quad \text{and} \quad P_q(q) = \int^q T_{qq}^{cl}(\bar{q}) d\bar{q} \quad (26)$$

are given functions of q , which are determined by the initial data on \mathfrak{S}_R^+ . Eq. (25) is a second order, non-linear, ordinary differential equation for the boundary curve $q(z)$. We solve it numerically for different profiles of the infalling matter using an embedded fifth-order Runge-Kutta ODE integration routine [27]. After obtaining $q(z)$ we use Eqs. (14) and (20) to find $T_{--}^{cl}(x^-)$ and $t_-(x^-)$ and integrate Eq. (10) to obtain the solution $X(x^+, x^-)$.

III. SOLUTIONS

A. Vacuum solutions

In this subsection we consider solutions of (25) with different profiles of infalling null matter. First consider the vacuum solutions, for which $T_{qq}^{cl}(q) = P_q(q) = 0$. The general

solution of (25) with $T_{qq}^{cl}(q) = P_q(q) = 0$ and the initial conditions $q(z \rightarrow -\infty) \rightarrow 0$ and $(dq/dz)(z \rightarrow -\infty) \rightarrow 0$, is

$$q_{vac}(z) = -\frac{a}{z}, \quad (27)$$

where a is some positive constant. One finds from (22) and (27) the one-parameter family of vacuum solutions

$$X_{vac}(x^+, x^-) = -\lambda^2 x^+ x^- - \frac{\kappa}{4} \ln(-\lambda x^+ x^-) + \frac{\kappa}{4} \ln(a) - a. \quad (28)$$

These are static solutions [10]. For $a > \kappa/4$ the solution (28) has a time-like singularity in the strong coupling region, $e^{2\phi} \rightarrow \infty$, while for $a < \kappa/4$ the solution has null singularities in the weak coupling region $e^{2\phi} \rightarrow 0$. The solution with $a = \kappa/4$ is everywhere regular, has the geometry of a semi-infinite throat, and can be regarded as the ground state of the theory [10]. One can show that [28] compared to this ground state, the ADM mass of the static solution in Eq. (28) is

$$M = \lambda \left[\frac{\kappa}{4} \ln \left(\frac{4a}{\kappa} \right) - \left(a - \frac{\kappa}{4} \right) \right]. \quad (29)$$

B. Smooth infalling matter

In the following we consider more general infalling matter with compact support, $x_1^+ < x^+ < x_2^+$. For $x^+ < x_1^+$, i.e., region I in Fig. 2, we have $T_{qq}^{cl} = P_q = 0$, and the solution is one of the vacuum solutions (28). If the total mass of the infalling matter, $M \equiv M(x^+ \rightarrow \infty)$ in Eq. (22), is above a critical value M_{cr} , then a black hole is formed. The critical mass M_{cr} is of the order of λa [10] and is determined numerically from the profile of the infalling matter stress-tensor and the ADM mass of the initial spacetime. We take $M/\lambda \gg \kappa$ for the validity of the semiclassical approximation [29]. Since we consider subcritical solutions in which a black hole does not quite form, a is at least of the order of M/λ and hence $a \gg \kappa$. We take $a = 1$ and $\kappa = 10^{-6}$. Our results would be similar for any values of a and κ as long as $a \gg \kappa$. We also fix the scale of the x^+ coordinate such that $\lambda x_1^+ = 1$. Define z_1 to be the value of $z = \lambda x^-$ in Eq. (25) corresponding to $q(z_1) = \lambda x_1^+$ (see Fig. 2). Using $\lambda x_1^+ = 1$, $a = 1$ and $X_B \approx 0^+$ we find from Eq. (28) that $z_1 = -1$. For $z < z_1$, i.e., in regions I, II and III in Fig. 2, the solution of Eq. (25) for $q(z)$ is given by Eq. (27), and the solution for $X(x^+, x^-)$ is

$$X(\lambda x^- < z_1) = -\lambda x^+ [\lambda x^- + \lambda^{-1} P_+(x^+)] - \frac{\kappa}{4} \ln(-\lambda^2 x^+ x^-) + \frac{M(x^+)}{\lambda}.$$

For $z \geq z_1 = -1$ (see Fig. 2) we have to integrate Eq. (25) numerically to find the boundary curve $q(z)$. So the range of z to be integrated numerically is $[-1, 0)$. The initial values for the numerical integration of the ODE (25) are (using (27) with $a = 1$): $q(z = z_1) = 1$ and $dq/dz(z = z_1) = 1$.

Before we give the results of our numerical integration, it is convenient to define coordinates in which the dynamical metric of our spacetime corresponding to the solution (21) is manifestly asymptotically flat on \mathfrak{S}_R^\pm . In the Kruskal coordinates, the metric is

$$ds^2 = -\exp[2\rho(x^+, x^-)]dx^+dx^- = -X^{-1}dx^+dx^- \quad , \quad (30)$$

where $X = \exp[-2\rho(x^+, x^-)]$ in these coordinates and is given by Eq. (21). The required asymptotically flat coordinates are (u, v) , defined in terms of the Kruskal coordinates by the following conformal coordinate transformation:

$$v = \lambda^{-1} \ln(\lambda x^+) \quad \text{and} \quad u = -\lambda^{-1} \ln(-\lambda x^- - P_+/\lambda) \quad , \quad (31)$$

where $P_+ = P_+(x^+ \rightarrow \infty)$ is the total momentum of the infalling matter. Rewriting the metric (30) in terms of the (u, v) coordinates shows that $\exp[2\rho(v, u)] \rightarrow 1$ as $v \rightarrow \infty$ on \mathfrak{S}_R^+ and $u \rightarrow -\infty$ on \mathfrak{S}_R^- .

Consider now the stress tensor describing a smooth profile of infalling matter:

$$T_{vv}^{cl}(v) = \begin{cases} 0 & , \quad v < 0 \\ (2M/\epsilon) \sin^2(\pi v/\epsilon) & , \quad 0 < v < \epsilon \\ 0 & , \quad v > \epsilon \end{cases} \quad (32)$$

where $v = \lambda^{-1} \ln(\lambda x^+)$. In Fig. 3a we show the profile (32). Here M is the total mass of the infalling matter, $M = \int_0^\infty T_{vv}^{cl}(v)dv$, and ϵ is its width.

To integrate (25) we need to write T_{qq}^{cl} in terms of q . Using (24) and (26) in (32), we get

$$T_{qq}^{cl}[q] = \begin{cases} 0 & , \quad \ln(q) < 0 \\ \frac{2M}{\lambda^2 \epsilon q^2} \sin^2(\pi \ln(q)/(\lambda \epsilon)) & , \quad 0 < \ln(q) < \lambda \epsilon \\ 0 & , \quad \ln(q) > \lambda \epsilon \end{cases} \quad (33)$$

We numerically solve (25) with (33) for different values of M/λ and $\lambda\epsilon$, and find the corresponding boundary curves $q(z)$ and solutions $X(x^+, x^-)$.

It is hard to extract physical information from the coordinate-dependent definition of the boundary curve. For example, as long as the boundary curve is everywhere timelike, one can define null coordinates $y^+ = x^+$ and $y^- = x_B^+(x^-)$ in which the boundary curve is ‘‘static’’, being given by the equation $y = 0$, where y is the spatial coordinate $y \equiv (y^+ - y^-)/2$. On the other hand a quantity giving physical insight into the nature of the solutions is the outgoing radiation reaching future asymptotic null infinity, \mathfrak{S}_R^+ . The outgoing radiation consists of a classical part (14) that is reflected from the boundary, and a quantum part (12). We calculate both in the manifestly asymptotically flat null coordinates on \mathfrak{S}_R^+ . In terms of the u coordinate defined in Eq. (31) we have on \mathfrak{S}_R^+ ,

$$T_{uu}^{cl}(u) = (\lambda x^- + P_+/\lambda)^2 T_{--}^{cl}(x^-(u)) \quad . \quad (34)$$

On the other hand, Eq. (12) gives

$$\langle T_{uu} \rangle(u) = -\kappa t_u(u) \quad , \quad (35)$$

where we used the fact that ρ and its derivatives vanish on \mathfrak{S}_R^+ in the manifestly asymptotically flat coordinates. Furthermore, using the coordinate transformation (31) and Eq. (16) with $x^+ \rightarrow x^-$ and $v \rightarrow u$, one can express $t_u(u)$ in terms of $t_-(x^-(u))$ to get

$$\langle T_{uu} \rangle(u) = (\kappa\lambda^2/4)[1 - \lambda^{-2}(\lambda x^- + P_+/\lambda)^2 t_-(x^-(u))] . \quad (36)$$

Putting the numerically integrated function $q(z)$ (defined in Eq. (24)) and the initial data, $T_{++}^{cl}(x^+)$, in (14) and (20), we find the profiles of the outgoing matter fluxes T_{uu}^{cl} and $\langle T_{uu} \rangle$. The results are shown in Fig. 4 (a) and (b) in which the infalling matter is described by the profile given in Eq. (32) with $\lambda\epsilon = 5$. In Fig. 4 (a), the mass is $M/\lambda = 0.1$ (which is 10% of a), while in Fig. 4 (b) it is $M/\lambda = 1$. The solid curves depict the total stress-tensor of the outgoing radiation, $T_{uu}^f = T_{uu}^{cl} + \langle T_{uu} \rangle$, in units of λ^2 , while the gray curves correspond to the quantum radiation stress-tensor, $\langle T_{uu} \rangle$. Since $\kappa = 10^{-6}$ is much smaller than M/λ , the quantum radiation is scaled up in the figures by a factor of $2/\kappa = 2 \times 10^6$ and hence does not show up in the solid curve.

As we will see later in section V, when the total mass and the local density of the infalling matter are large enough, then a black hole is formed; otherwise the infalling matter escapes to infinity without forming a black hole. For a fixed width ϵ in Eq. (32), the mass of the infalling matter M fully determines its profile. Let M_{cr} be the mass above which a black hole is formed. As discussed in section V, for $\lambda\epsilon = 5$, we find that $M_{cr}/\lambda \simeq 1.5$. In Fig. 4 (a), we take the mass of the infalling matter to be about 6% of the critical mass M_{cr} . We see that the total outgoing radiation is very similar to the incoming radiation, Fig. 3a. The profile of the matter field is almost unaffected by the evolution. The curvature and coupling are everywhere small and the infalling matter is just reflected from the boundary with almost no distortion. In the 4D case, this corresponds to “weak” initial data [30] for which the null (scalar) field goes through the origin of the radial coordinate, $r = 0$, without developing large densities, and escapes to infinity with very little distortion.

The quantum part of the outgoing radiation stress-tensor $\langle T_{uu} \rangle$ in Fig. 4a is almost symmetric. (This is true only for a symmetric incoming classical profile far from the critical point.) The quantum radiation includes a region of negative-energy density that insures energy conservation. In section IV we will calculate the quantum correlation function and show that the negative-energy radiation is strongly correlated with the positive-energy radiation. This strong correlation is necessary for the quantum state on \mathfrak{S}_R^+ to be pure.

In Fig. 4 (b) the mass of the infalling matter is about 65% of the critical mass M_{cr} . We see that the outgoing classical radiation is more distorted compared to that in Fig. 4 (a). In this case the infalling matter strongly distorts the spacetime before getting reflected from the boundary and escaping to infinity without forming a black hole. Likewise the quantum radiation in Fig.4(b) is no longer symmetric. The reason for this is the following: As M increases, the total amount of positive-energy quantum radiation increases. Because of energy conservation also the total amount of negative-energy radiation increases with M . While the width of the positive-energy radiation increases with M , the width of the negative-energy radiation, Δu , satisfies the quantum inequality [15,31]

$$|E_{neg}| \Delta u < \kappa , \quad (37)$$

where E_{neg} is the total amount of negative-energy quantum radiation and Δu is its width (as measured by an asymptotic observer). Since $|E_{neg}|$ increases with M , the width Δu must

decrease and we get a non-symmetric profile of $\langle T_{uu} \rangle$. As we will see in section V, as M approaches M_{cr} the width Δu approaches zero, and we get a brief burst of negative energy.

As a consequence of general covariance of the effective action, Eq. (1), we have $\nabla^\mu T_{\mu\nu}^f = 0$. We find numerically that the energy defined in terms of $T_{\mu\nu}^f$ is conserved, i.e., $\int_{\mathfrak{S}_R^-} T_{vv}^f dv = \int_{\mathfrak{S}_R^+} T_{uu}^f du$. This is what one would expect if the reflecting boundary at $X \equiv \exp(-2\phi) = 0^+$ corresponds to a static boundary like $r = 0$ in 4D, as discussed in the paragraph after Eq. (18). The \hbar expansion implies that also $\nabla^\mu T_{\mu\nu}^{cl} = 0$ and $\nabla^\mu \langle T_{\mu\nu} \rangle = 0$ (the latter was used in arriving at $\langle T_{\mu\nu} \rangle$ from the trace anomaly). Nevertheless, we find numerically that the energies associated with the classical and quantum parts alone are not separately conserved. For example, $\int_{\mathfrak{S}_R^-} T_{vv}^{cl} dv \neq \int_{\mathfrak{S}_R^+} T_{uu}^{cl} du$. Evidently, because the total energy-momentum tensor, $T_{\mu\nu}^f$, determines ϕ , and hence the boundary, it behaves like a static boundary only for $T_{\mu\nu}^f$ but not for $T_{\mu\nu}^{cl}$ or $\langle T_{\mu\nu} \rangle$ individually. Far below criticality, the classical and quantum parts of the energy are nearly conserved separately. However, as one approaches the critical solution the classical and quantum parts of the energy each are strongly non-conserved.

Next we consider the profile described by

$$T_{vv}^{cl}(v) = \begin{cases} 0 & , & v < 0 \\ \frac{M}{(v_0+\epsilon/2)} \sin^2(\pi v/\epsilon) & , & 0 < v < \epsilon/2 \\ \frac{M}{v_0+\epsilon/2} & , & \frac{\epsilon}{2} < v < v_0 + \frac{\epsilon}{2} \\ \frac{M}{(v_0+\epsilon/2)} \sin^2[\pi(v - \lambda v_0)/\epsilon] & , & v_0 + \frac{\epsilon}{2} < v < v_0 + \epsilon \\ 0 & , & v > v_0 + \epsilon . \end{cases} \quad (38)$$

In Fig. 3(b) we show the profile (38) with $v_0/\epsilon = 100$, which is nearly a square waveform. For $v_0 \gg \epsilon$, as shown in Fig. 3(b), the energy-momentum tensor (38) describes infalling matter of nearly homogeneous density. The total width of the profile is $(v_0 + \epsilon)$. In terms of the q -coordinate defined in Eq. (24), the profile (38) is

$$T_{qq}^{cl}[q] = \begin{cases} 0 & , & \ln(q) < 0 \\ \frac{M}{\lambda^2(v_0+\epsilon/2)q^2} \sin^2[\pi \ln(q)/(\lambda\epsilon)] & , & 0 < \ln(q) < \lambda\epsilon/2 \\ \frac{M}{\lambda^2(v_0+\epsilon/2)q^2} & , & \lambda\epsilon/2 < \ln(q) < \lambda(v_0 + \frac{\epsilon}{2}) \\ \frac{M}{\lambda^2(v_0+\epsilon/2)q^2} \sin^2\{\pi[\ln(q) - \lambda v_0]/(\lambda\epsilon)\} & , & \lambda(v_0 + \frac{\epsilon}{2}) < \ln(q) < \lambda(v_0 + \epsilon) \\ 0 & , & \ln(q) > \lambda(v_0 + \epsilon) . \end{cases} \quad (39)$$

We take (39) with $\lambda v_0 = 10$ and $\lambda\epsilon = 0.1$, and integrate (25) for different values of M/λ . Using the numerically integrated function, $q(z)$, we calculate the outgoing classical and quantum radiation on \mathfrak{S}_R^+ , shown in Fig. 4 (c) and (d). In (c) we take $M/\lambda = 0.1$ and in (d) $M/\lambda = 2$. Because the mass distribution of (38) is more spread out than that of (32), M_{cr} is larger, having the value $M_{cr}/\lambda \simeq 3.0$. In these figures, the solid curves describe the total radiation while the gray curves describe the quantum radiation scaled up by 2×10^6 . In Fig. 4c the mass is about 3% of the critical mass, which is the case of weak initial data, and is similar to Fig. 4a. The total outgoing radiation is very similar to the incoming classical radiation, Fig. 3(b), and the quantum radiation is spread across the outgoing classical radiation symmetrically. In Fig. 4d the mass is about 65% of the critical mass, as was the case in Fig. 4b. The outgoing radiation is more distorted and the quantum radiation is non-symmetric.

Finally, recall that in Ref. [15] the case in which the classical matter had the form of an incoming shock-wave was studied. To recover the results of Ref. [15], consider profiles (32) with $M/\lambda = 0.1$ but with different values of the width $\lambda\epsilon$. In Fig. 5, the curves a and α are, respectively, the total and quantum outgoing radiation in the case $\lambda\epsilon = 5$. The curves b and β are the total and quantum outgoing radiation for $\lambda\epsilon = 1$, and c and γ correspond to $\lambda\epsilon = 0.1$. One can see that as $\lambda\epsilon$ becomes smaller, the (incoming and outgoing) classical radiation becomes very localized, while the transition of the quantum radiation from positive to negative-energy values becomes more sudden. In the limit $\lambda\epsilon \rightarrow 0$, the classical energy-momentum tensor can be described by a delta function $T_{++}^{cl} = (M/\lambda x_0^+) \delta(x^+ - x_0^+)$ and one recovers the results of Ref. [15]. One should remember however that as $\lambda\epsilon \rightarrow 0$, the derivative p' in Eq. (15) diverges, and the large N limit should be taken in such a way that the second term on the right-hand-side of Eq. (15) can be neglected [15].

IV. INFORMATION

A. Classical Structure

In section III we considered infalling matter with very little structure. In order to encode non-trivial information in the classical infalling matter one should consider more complicated profiles. For example one can encode information in bits. In this case the infalling null matter can be a sequence of pulses each corresponding to one bit of information. Let us send a message in binary numbers. The number “1” is described by a pulse of relative height 1 and “0” by a pulse of relative height 0.5. As an example consider the following incoming energy-momentum tensor

$$T_{vv}^{cl}(v) = \sum_{i=1}^{16} l_i \Theta_i(v), \quad (40)$$

where

$$\Theta_i(v) = \begin{cases} \frac{20M}{11} \sin^2[10\pi(v - i)] & , \quad i < v < i + 0.1 \\ 0 & , \quad \text{elsewhere} , \end{cases} \quad (41)$$

and

$$l_i \in \{0.5, 1, 0.5, 0.5, 1, 0.5, 0.5, 0.5, 0.5, 1, 1, 0.5, 1, 0.5, 0.5, 1\}. \quad (42)$$

In Fig. 3c we show the profile (40). It corresponds to the binary number 0100100001101001, which is the word “Hi” in ASCII. In the q -coordinate the profile (40) is

$$T_{qq}^{cl}[q] = \sum_{i=1}^{16} l_i \Theta_i(q), \quad (43)$$

where

$$\Theta_i(q) = \begin{cases} \frac{20M}{11\lambda q^2} \sin^2\{10\pi[\ln(q) - i]\} & , \quad i < \ln(q) < i + 0.1 \\ 0 & , \quad \text{elsewhere} . \end{cases} \quad (44)$$

Using (43), we integrate (25) for different values of M/λ and find $q(z)$. Then we calculate the classical and quantum radiation on \mathfrak{S}_R^+ , shown in Fig. 6. In (a) we take $M/\lambda = 0.1$, and in (b) we take $M/\lambda = 2$. The solid curves describe the total outgoing radiation, while the gray curves describe the quantum radiation, scaled by $2/\kappa = 2 \times 10^6$.

For the profile (40), we find numerically that the critical mass is $M_{cr}/\lambda \simeq 2.5$. In Fig. 6a the mass is about 4% of the critical mass, and indeed we see that the outgoing radiation is very similar to the incoming one, Fig. 3c. This case is similar to the ones in Fig. 4a and 4c. One can easily recover the ‘‘classical information’’, (the word ‘‘Hi’’), from the outgoing radiation in Fig. 6a. Also the quantum radiation is quite symmetric. We can see from Fig. 6a that the classical and quantum radiation are correlated. Actually one can recover the ‘‘classical information’’ from the quantum radiation alone. Each classical pulse results in a sharp decrease (‘‘jump’’) of the quantum radiation. We see that for a pulse of a relative height 1 the jump is twice as large as the jump for a pulse of a relative height 0.5. Therefore by looking at the different jumps in the quantum radiation one can recover the ‘‘classical information’’.

In Fig. 6b the mass is about 80% of the critical mass, and the outgoing radiation is much more distorted than in Fig. 6a. As in the cases shown in Fig. 4b and 4d, it is difficult to recover the ‘‘classical information’’ of Fig. 3c from the profile shown in Fig. 6b.

B. Quantum correlation function

As discussed earlier in section II, we choose the quantum state to be the vacuum on \mathfrak{S}_R^- , so that the quantum contribution to the energy-momentum tensor on \mathfrak{S}_R^- is always zero, $\langle T_{vv} \rangle(v) = 0$. By construction (with the reflecting boundary conditions and no black hole formation), the evolution of the quantum state must be unitary. How can we see that the quantum radiation on \mathfrak{S}_R^+ is described by a pure state? The created quantum radiation reaching \mathfrak{S}_R^+ before the escaping classical matter is the beginning of the Hawking radiation which is almost thermal and by itself does not correspond to a pure state. A pure state can be recovered from the radiation on \mathfrak{S}_R^+ only if there are strong correlations between the early-time Hawking radiation and late-time negative-energy radiation reaching \mathfrak{S}_R^+ after the escaping outgoing classical matter. We demonstrate these correlations by calculating the correlation function

$$C_{\mu\nu,\mu'\nu'}(x, x') \equiv \langle \hat{T}_{\mu\nu}^f(x) \hat{T}_{\mu'\nu'}^f(x') \rangle - \langle \hat{T}_{\mu\nu}^f(x) \rangle \langle \hat{T}_{\mu'\nu'}^f(x') \rangle. \quad (45)$$

The correlations between different points u and u' on \mathfrak{S}_R^+ are given by $C_{uu,u'u'}(u, u')$, where u is the asymptotically flat null coordinate on \mathfrak{S}_R^+ . For the reflecting boundary conditions, we have a closed form expression¹ [32]

$$C_{uu,u'u'}(u, u') = \frac{N\hbar^2 (\partial_u v_B(u))^2 (\partial_{u'} v_B(u'))^2}{8\pi (v_B(u) - v_B(u'))^4}, \quad (46)$$

¹In Ref. [15], the factor $N\hbar^2$ did not appear explicitly in Eq. (6) of Ref. [15] and the values of $C_{--,--}(u, u')$ quoted there are in units of $N\hbar^2$.

where $v_B(u)$ is the boundary curve in the (u, v) coordinates defined in Eq. (31). Using the numerical solution for $q(z)$, we numerically find the functions $v_B(u) = \lambda^{-1} \ln\{q[z(u)]\}$ and $\partial_u v_B(u)$, and from there can obtain $C_{uu, u'u'}(u, u')$.

The denominator in Eq. (46) is a rapidly varying function of u and u' . By defining the relative correlation

$$\frac{C(+)}{C(-)} \equiv \frac{C_{uu, u'u'}(u, u')}{C_{u''u'', u'u'}(u'', u')} \quad , \quad \text{where} \quad v_B(u) - v_B(u') = v_B(u') - v_B(u'') \quad , \quad (47)$$

we get a measure for the correlations that varies more slowly as a function of u and u' and also is not proportional to \hbar , which we take to be very small in the large N limit. This relative correlation is plotted as a function of u , with u' held fixed. The numerical results for the relative correlations (47) and the outgoing quantum radiation shown in Fig. 4a, when we fix $\lambda u' = 0$, are shown in Fig. 7a. Since for $u < 0$ the quantum radiation in Fig. 4a is exponentially small, the correlation function $C(-)$, which describes the correlations between the radiation at $u = 0$ and the radiation at $u < 0$, is approximately the vacuum correlation function (there are almost no created particles in this region). On the other hand, the correlation function $C(+)$ describes the correlations between the radiation at $u = 0$ and the radiation at $u > 0$. Since most of the radiation is in the region $u > 0$, we can regard $C(-)$ as a reference function relative to which $C(+)$ is being measured. If $C(+)/C(-) < 1$, then the correlations described by $C(+)$ are weaker than the vacuum correlations, while if $C(+)/C(-) > 1$, then the correlations are stronger.

We see from Fig. 7a that when u is in the region of positive-energy radiation (see also Fig. 4a), we have $C(+)/C(-) < 1$. This is expected since the positive-energy radiation is the precursor of the uncorrelated thermal Hawking radiation. On the other hand, for u in the region of negative-energy radiation we have $C(+)/C(-) > 1$. Namely, the correlations between a point in the region of positive-energy radiation, i.e., at $u = 0$, and a point in the region of negative-energy radiation are *stronger* than the vacuum correlations. It is just when the energy of the quantum radiation becomes negative that $C(+)/C(-)$ becomes greater than one. Hence, the negative-energy radiation is not only necessary for energy conservation, but is also instrumental in recovering the correlations present in the final pure state. Before we can discuss what happens to information when M is very near the critical mass M_{cr} , we must study the properties of the near-critical spacetimes.

V. NEARLY CRITICAL SPACETIMES

A. Approaching the critical solutions

The reflecting boundary conditions can only be imposed on those sections of the boundary curve that are timelike. Along these sections, the boundary curve can be written in the form $x^+ = x_B^+(x^-)$, where $x_B^+(x^-)$ is a well-defined function, and one can impose the condition (13). Since the boundary curve is dynamical, the initial data determines its nature through the evolution equations. If the boundary is everywhere timelike, then the general solution we found earlier is regular, energy-conserving, and unitary. Such a solution is called a subcritical (i.e., a non-black hole) solution. If on the other hand the boundary becomes spacelike in

some regions of spacetime, then the spacetime develops a spacelike singularity [10], which is initially hidden behind an apparent horizon. Such a solution is called a supercritical solution and describes an evaporating black hole [10]. One can therefore distinguish between two regions in the space of solutions or the space of initial data: black hole and non-black hole solutions. Furthermore, one can find continuously varying parameters p_i , specifying the initial data, such that all solutions with $p_i < p_i^*$ are subcritical, while all solutions with $p_i > p_i^*$ are supercritical. The solutions on the boundary separating the two regions (i.e., the ones with $p_i = p_i^*$) are called the critical solutions. As a result of the non-linearity of the system, the physical properties of the solutions need not be continuous functions of the parameters at the critical values p_i^* .

We would like to study the transition between the subcritical and supercritical regions in our semiclassical theory. Using our numerical integration we can easily determine whether the solution is subcritical or supercritical: As long as the boundary curve is timelike we can write the boundary equation, $x^+ = x_B^+(x^-)$, in the inverse form $x^- = x_B^-(x^+)$, where x_B^- is the inverse function of x_B^+ . Since the boundary is smooth, the quantity $\partial x_B^-/\partial x^+$ is continuous. For a timelike boundary $\partial x_B^-/\partial x^+$ is positive, for a spacelike boundary $\partial x_B^-/\partial x^+$ is negative, and for a null boundary $\partial x_B^-/\partial x^+ = 0$. So at the point where the initially timelike boundary becomes null, just before becoming spacelike, the derivative dq/dz in Eq. (25) (which is the inverse of $\partial x_B^-/\partial x^+$) *diverges* and the numerical integration terminates. Therefore, all solutions for which the integration terminates at a finite value of x_B^+ are supercritical, while the others are subcritical.

For the profiles in Fig. 3 the continuous dimensionless parameters in solution space are: M/λ and $\lambda\epsilon$ in case (a), M/λ , $\lambda\epsilon$ and λv_0 in case (b), and M/λ (the l_i are not continuous parameters) in case (c). We approach the critical solutions by varying one of the parameters, while keeping the others fixed. First we take $m \equiv M/\lambda$ to be the free parameter. In case (a) we fix $\lambda\epsilon = 5$, and in case (b) we fix $\lambda\epsilon = 0.1$, $\lambda v_0 = 10$. We find that in all the above cases there exists a critical value m^* such that if $m < m^*$ the solutions are subcritical while if $m > m^*$ the solutions are supercritical. The value of m^* depends on the values of the fixed parameters. To study the behavior of the solutions just below criticality, we numerically integrate the boundary equation for the cases $0 < \Delta m/m^* \ll 1$, where $\Delta m \equiv m^* - m$. We take $\kappa = 10^{-2}$ in this section, in order to be able to easily probe the regime, $\Delta m \leq \kappa$. (The values of m near m^* are of order 1 and thus are still large with respect to κ .) Then we calculate the outgoing radiation on \mathfrak{S}_R^+ . In Fig. 8 we show the radiation on \mathfrak{S}_R^+ for the three cases (a), (b) and (c) of Fig. 3, where $\Delta m/m^* \sim 10^{-5}$. We shift the u -coordinate to $u - u_*$, where u_* corresponds to the last classical reflected null ray, (i.e., $u_* = \lambda^{-1} \ln[-\lambda x_B^-(x_2^+) - P_+/\lambda]$). In Fig. 8a we show the total stress tensor, T_{uu}^f , in units of λ^2 , describing the outgoing radiation on \mathfrak{S}_R^+ , and in Fig. 8b we show only the quantum part. The quantum radiation is scaled by $4/(\kappa\lambda^2)$, such that $\langle T_{uu} \rangle = 1$ corresponds to the constant Hawking radiation from a 2D black hole [19].

We see from Fig. 8 that while the early-time radiation strongly depends on the details of the classical infalling matter, the late-time radiation in the region $u > u_* - \lambda^{-1}$ is almost the same for all the cases (a), (b) and (c). In the region $u > u_* - \lambda^{-1}$ the classical part, T_{uu}^{cl} , increases rapidly to large values of the order of $10^8\lambda^2$, and then sharply decreases to zero. The quantum part, $\langle T_{uu} \rangle$, approaches the constant Hawking radiation, $\langle T_{uu} \rangle = \kappa\lambda^2/4$, just before $u = u_*$. It then decreases rapidly to negative values of the order of $-10^8\lambda^2$, and

finally increases rapidly to zero. This late-time behavior appears to be independent of the profile of the infalling matter, as long as $0 < \Delta m/m^* \ll 1$. Similarly, if we approach a critical solution by varying any one of the other parameters p , while holding the rest fixed, we find the same late-time behavior as long as $0 < (p^* - p)/p^* \ll 1$. Let T_{max} and T_{min} be the maximum and minimum values of the total radiated energy flux T_{uu}^f on \mathfrak{S}_R^+ . For all the cases that we studied we find numerically that as $(p^* - p)/p^* \rightarrow 0^+$, the value of T_{min} approaches $-T_{max}$ and T_{max} tends to infinity. In the next subsection we analyze this critical behavior.

B. Breakdown of the semiclassical approximation ?

To understand the above late-time behavior analytically, we write $T_{uu}^{cl}(u)$ and $\langle T_{uu}(u) \rangle$ explicitly, using (14) and (36),

$$T_{uu}^{cl}(u) = \left(\frac{\partial x^-}{\partial u} \right)^2 \times \left(\frac{\partial x_B^+(x^-)}{\partial x^-} \right)^2 \times T_{++}^{cl}(x_B^+) \quad (48)$$

and

$$\langle T_{uu}(u) \rangle = \frac{\kappa \lambda^2}{4} \left[1 - \frac{1}{(\lambda x_B^+)^2} \left(\frac{\partial x^-}{\partial u} \right)^2 \left(\frac{\partial x_B^+(x^-)}{\partial x^-} \right)^2 \right]. \quad (49)$$

We take the classical stress-tensor describing the incoming matter, T_{++}^{cl} , to be everywhere regular, i.e., finite and smooth. Therefore the non-trivial contributions to (48) and (49) come from the ‘‘redshift factor’’, $(\partial x^-/\partial u)^2$, or from the ‘‘blueshift factor’’, $(\partial x_B^+/\partial x^-)^2$. Consider first the redshift factor. From the coordinate transformation (31) we get $(\partial x^-/\partial u)^2 = \exp(-2\lambda u)$. If we ignore the back-reaction, i.e., take $\kappa = 0$ as explained in [29], the boundary curve of the critical solution first becomes null as $u \rightarrow \infty$, and the redshift factor approaches zero. However, when we include the back-reaction, the redshift factor at the point where the boundary becomes null is finite, as can be seen as follows. Let (x_c^+, x_c^-) be the point at which the boundary curve becomes null. At that point an apparent horizon is formed, since when the boundary curve becomes space-like (and describes a black hole singularity) it is surrounded by an apparent horizon [10]. The equation for the apparent horizon is $\partial e^{-2\phi}/\partial x^+ = 0$ [26], and using (21) we get

$$-\lambda x_{\text{ah}}^-(x^+) = P_+(x^+)/\lambda + \frac{\kappa}{4\lambda x^+}, \quad (50)$$

where the apparent horizon curve is $x^- = x_{\text{ah}}^-(x^+)$. Defining $\Delta P_+ = P_+(x^+ \rightarrow \infty) - P_+(x_c^+)$ and using (31) and (50), we find at (x_c^+, x_c^-)

$$\left(\frac{\partial x^-}{\partial u} \right)_{x_c^-}^2 = \left(\frac{\kappa}{4\lambda x_c^+} - \frac{\Delta P_+}{\lambda} \right)^2. \quad (51)$$

Note that the apparent horizon is null at (x_c^+, x_c^-) . This can be seen by showing that the derivative of (50) with respect to x^+ vanishes at the point (x_c^+, x_c^-) on the boundary $X = 0$,

where X is given by Eq. (21). From the definition $P_+(x^+) = \int dx^+ T_{++}^{cl}(x^+)$ and the fact that $\partial x_{\text{ah}}^- / \partial x^+ = 0$ at (x_c^+, x_c^-) , we get

$$T_{++}^{cl}(x_c^+) = \frac{\kappa}{(2x_c^+)^2}. \quad (52)$$

It follows that $T_{vv}^{cl}(v(x_c^+))$ is of order $\kappa\lambda^2$, which is the same as the quantum contribution. Therefore, x_c^+ must be close to the cut-off point x_2^+ of the classical matter distribution (the location of x_2^+ is shown in Fig. 2, assuming that the profile $T_{vv}^{cl}(v)$ has no anomalously long tail. Expanding $\Delta P_+ \simeq (\partial P_+ / \partial x^+) \Delta x^+ = T_{++}^{cl}(x^+) \Delta x^+$, where $\Delta x^+ \equiv x_2^+ - x_c^+ \ll x_c^+$, and using (50)-(52) we finally get

$$\left(\frac{\partial x^-}{\partial u} \right)_{x_c^-}^2 \simeq \left(\frac{\kappa}{4\lambda x_c^+} \right)^2 \left(1 - \frac{2\Delta x^+}{x_c^+} \right) \simeq \left(\frac{\kappa}{4\lambda x_c^+} \right)^2. \quad (53)$$

Thus the redshift factor (53) is finite at (x_c^+, x_c^-) , and is zero only if we neglect the back-reaction ($\kappa = 0$).

Next consider the blueshift factor, $(\partial x_B^+ / \partial x^-)^2$. Obviously when the boundary curve becomes null the blueshift factor diverges. This divergence, together with the finiteness of the redshift factor and T_{++}^{cl} , is the reason for the divergences in (48) and (49) at $u_c \equiv u(x_c^-)$. But what about the total stress-tensor, $T_{uu}^f = T_{uu}^{cl} + \langle T_{uu} \rangle$? From (48), (49), and (52) we see that at (x_c^+, x_c^-) the diverging terms in T_{uu}^{cl} and $\langle T_{uu} \rangle$ cancel each other, leaving a finite T_{uu}^f :

$$T_{uu}^f(u_c) = \frac{\kappa\lambda^2}{4}. \quad (54)$$

So why do we get divergences in the total stress tensor, shown in Fig. 8a? To understand this behavior, consider a point $(x_0^+, x_0^- = x_B^-(x_0^+))$ near (x_c^+, x_c^-) on the boundary of a critical solution. Defining $\delta \equiv x_c^+ - x_0^+$ and expanding (48), (49) about (x_c^+, x_c^-) to leading orders in δ , dropping the finite term (54), we find

$$T_{uu}^f(u_0) \simeq - \left(\frac{\kappa}{4\lambda x_c^+} \right)^2 \left[\frac{\kappa}{2(x_c^+)^3} + \left(\frac{\partial T_{++}^{cl}}{\partial x^+} \right)_{x_c^+} \right] \frac{\delta}{(a\delta + b\delta^2)^2}, \quad (55)$$

where $a \equiv [\partial^2 x_B^- / \partial (x^+)^2]_c$, $b \equiv [\partial^3 x_B^- / \partial (x^+)^3]_c$, and $u_0 = u(x_0^-)$. The point (x_c^+, x_c^-) cannot be a local maximum of the boundary curve, since the boundary curve of the critical solution never becomes space-like. It also cannot be a local minimum since by construction it is the first (and only) point at which the boundary is null. Therefore the point (x_c^+, x_c^-) must be an inflection point, i.e., $a = 0$. Also, for a general critical solution we have $(\partial T_{++}^{cl} / \partial x^+)_{x_c^+} < -\kappa / [2(x_c^+)^3]$, which is necessary for the apparent horizon in (50) to become timelike beyond the point (x_c^+, x_c^-) . We therefore get from (55) that $T_{uu}^f(u_0) \simeq A\delta^{-3}$ with $A > 0$. For points on the boundary to the past of x_c^+ , $T_{uu}^f \simeq +A|\delta|^{-3}$ and for points to the future of x_c^+ , $T_{uu}^f \simeq -A|\delta|^{-3}$ as $|\delta| \rightarrow 0$. Thus for critical solutions the radiation flux diverges in opposite ways on both sides as $x^+ \rightarrow x_c^+$. For almost critical solutions one gets the nearly divergent results shown in Fig. 8.

The fact that T_{uu}^f diverges does not necessarily signal a breakdown of the semiclassical approximation in which the metric and dilaton fields are treated as classical dynamical fields.

From conservation of energy we know that the total amount of outgoing radiation (the sum of positive and negative parts), is finite and equals the total amount of incoming radiation. Moreover, the total amount of positive-energy radiation alone, E_+ , in the region between x_c^- and x_0^- on \mathfrak{S}_R^+ , is proportional to $T_{max}\Delta x^-$, where $\Delta x^- \equiv x_c^- - x_0^-$. From $x_c^+ - x_0^+ = \delta$, we find that $\Delta x^- = b\delta^3$. It then follows from Eq. (55) that E_+ is finite. The same holds for the total amount of negative-energy radiation. Thus the divergence in the density, T_{uu}^f , can be viewed as describing a “shock wave” or “thunderpop” [9]. Although a shock wave does not necessarily imply a breakdown of the semiclassical approximation, an examination of the fluctuations in $\hat{T}_{\mu\nu}^f$ provides strong evidence for such a breakdown. Let us calculate the fluctuations in $\hat{T}_{\mu\nu}^f$. As an estimate for the fluctuations one can use the quantity [33,34]

$$\Delta'_{\mu\nu\mu'\nu'}(x, x') \equiv \left| \frac{\langle \hat{T}_{\mu\nu}^f(x) \hat{T}_{\mu'\nu'}^f(x') \rangle - \langle \hat{T}_{\mu\nu}^f(x) \rangle \langle \hat{T}_{\mu'\nu'}^f(x') \rangle}{\langle \hat{T}_{\mu\nu}^f(x) \rangle \langle \hat{T}_{\mu'\nu'}^f(x') \rangle} \right| = \left| \frac{C_{\mu\nu,\mu'\nu'}(x, x')}{\langle \hat{T}_{\mu\nu}^f(x) \rangle \langle \hat{T}_{\mu'\nu'}^f(x') \rangle} \right|. \quad (56)$$

Far below criticality, with x and x' sufficiently apart, the numerator in Eq. (56) will be less than or of the order of $N\hbar^2$ (see Eq. (46)). On the other hand, the denominator is of the order of $\kappa^2 = N^2\hbar^2$. Hence, in this case the fluctuations (56) will be of the order of $1/N$ even in the region of negative energy. In the large N limit these fluctuations are small and the semiclassical approximation is valid. However, for critical or nearly critical solutions this is no longer the case. Let us estimate $\Delta'_{uuu'u'}(u, u')$ for a critical or nearly critical solution, with u and u' sufficiently far apart that $v_B(u) - v_B(u') \sim \lambda^{-1}$, which sets a natural length scale. Let u' approaches u_c , and take u to be in the region of negative energy such that $v_B(u) - v_B(u') \sim \lambda^{-1}$, which is consistent with the quantum inequality (37). Then using (46), (49), (54) and (56), we get for $u' \rightarrow u_c$

$$\Delta'_{uuu'u'}(u, u') \sim \frac{1}{N} \left(\frac{\partial v_B(u')}{\partial u'} \right)_{u' \rightarrow u_c}^2. \quad (57)$$

For any given N , no matter how large, while keeping u fixed, we can find u' sufficiently close to u_c such that the blueshift factor, $(\partial v_B/\partial u)^2$, in (57) is dominant over N , and the fluctuations (57) are large. We regard this anomalous behavior as implying a breakdown of the semiclassical approximation at criticality. Unlike in the 4D case, where the temperature of the black hole formed just above criticality approaches infinity, in the 2D case the black hole temperature is always a finite constant, $T_{BH} = \lambda/2\pi$, but nevertheless the semiclassical approximation (even in the large N limit) breaks down at criticality. Also, for the critical solution the quantity $p' = \partial x_B^+/\partial x^-$ diverges at x_c^- , and dropping the last term on the r.h.s. of Eq. (15), i.e., the moving mirror term, becomes problematic even in the large N limit.

VI. HIGH DENSITIES OF INFORMATION

A. Quantum limitations on the negative-energy radiation

Let us calculate the relative-correlation function (47) for nearly critical solutions. As in Fig. 7a, we take the infalling matter to be the one shown in Fig. 3a, with $\lambda\epsilon = 5$, but while

in Fig. 7a we take $\Delta m/m \sim 0.9$, in this section we take $\Delta m/m \sim 10^{-5}$. The results for the relative correlations are shown in Fig. 7b. We see that in the region of the Hawking radiation ($0 < \lambda u < 10.5$) the relative correlations are very small. Then in the region of the brief burst of negative energy, the relative correlations increase sharply to extremely high values of the order of 10^{11} , and sharply decrease to one. It is this sharp increase in the relative correlations that insure a unitary evolution. If it were not for the negative-energy burst the correlations would be lost and the final state would be a mixed state.

The information encoded in these correlations is very dense as the burst of negative energy is very localized (see Fig. 8a). To find an upper bound on the duration of the negative-energy burst, Δu , we use the quantum inequality (37). To estimate the value of $|T_{uu}^f|$, we use the analytic expressions (48), (49) for a nearly critical solution. The quantity $|E_{\text{neg}}|$ is approximately of the order of

$$|E_{\text{neg}}| \sim |(T_{uu}^f)_{\min}| \Delta u \simeq (T_{uu}^f)_{\max} \Delta u . \quad (58)$$

From (48) and (49) one can see that $(T_{uu}^f)_{\max}$ corresponds to the maximum of $\partial x_B^+ / \partial x^-$. Let (x_m^+, x_m^-) be the point on the boundary curve for which T_{uu}^f is maximum. Using the boundary equation $X(x^+, x_B^-) = X_B$ and the solution (21) we find that at the maximum of $\partial x_B^+ / \partial x^-$

$$T_{++}^{cl}(x_m^+) = \frac{\kappa}{2(x_m^+)^2} . \quad (59)$$

From (48), (49), (53), and (59) we find that for a nearly critical solution (for which $(\partial x_B^- / \partial x^+)_{\min}$ is very small)

$$(T_{uu}^f)_{\max} \simeq \frac{\kappa^3}{64\lambda^2(x_m^+)^4} \left(\frac{\partial x_B^-}{\partial x^+} \right)_{\min}^{-2} . \quad (60)$$

From (58), (60) and the quantum inequality (37), we get

$$\Delta u \leq \frac{8\lambda(x_m^+)^2}{\kappa} \left(\frac{\partial x_B^-}{\partial x^+} \right)_{\min} . \quad (61)$$

Since $x_m^+ < x_2^+$ is finite, as one approaches the critical solution $(\partial x_B^- / \partial x^+)_{\min}$ approaches zero and so does Δu . If the amount of information, ΔI , carried by this burst of negative energy is finite, then as we approach the critical solution the information density, $\dot{I} = \Delta I / \Delta u$, diverges. In the next subsection we show that this is indeed the case.

B. Entropy and Information

The results regarding the quantum part of the energy-momentum tensor discussed in the previous sections may plausibly be interpreted as arising from the creation of particle-antiparticle pairs [35]. The particles reach infinity, \mathfrak{S}_R^+ , and give rise to the positive-energy (Hawking) radiation, while the antiparticles carrying negative energy are reflected from the boundary and give rise to the negative-energy radiation on \mathfrak{S}_R^+ . If it were not for the negative-energy burst of radiation, the correlations between the particles and antiparticles, shown

explicitly in Fig. 7, would be lost and the final state would be a mixed state with non-zero entropy. The entropy of this mixed state can be found using the fact that the spectrum of the outgoing positive-energy quantum radiation is almost thermal, as can be seen by calculating the corresponding Bogolubov coefficients [36]. The entropy of this thermal radiation is the dimensionless Boltzmann entropy [21]

$$S_{\text{Bol}} = 2\hbar^{-1}\sqrt{\kappa} \int_{-\infty}^{u_0} \sqrt{\mathcal{E}(u)} du , \quad (62)$$

where \mathcal{E} is the energy density of the thermal quantum radiation, $\mathcal{E} = \langle T_{uu} \rangle$, and u_0 is the value of u at which the thermal radiation ends. From Fig. 8b we see that as we approach the critical solution, the thermal quantum radiation is almost independent of the specific profile of the infalling matter. Therefore to get an estimate of (62) one can calculate it for the case of very localized infalling matter. In that case one finds analytically that \mathcal{E} is given by [15]

$$\mathcal{E} = \frac{\kappa\lambda^2}{4} \left(1 - \frac{1}{(1 + \lambda\Delta e^{\lambda u})^2} \right) , \quad (63)$$

where $\Delta \equiv M/(\lambda^3 x_0^+)$, and $x^+ = x_0^+$ is the null trajectory of the localized (shock-wave) infalling matter. Then the Boltzmann entropy of the thermal radiation is

$$S_{\text{Bol}} \simeq \frac{N}{6} \ln \left(\frac{4M}{\lambda\kappa} \right) , \quad (64)$$

where we assume that $\ln(4M/\lambda\kappa) \gg 1$. The entropy (64) is by definition the amount of information that is lost by ignoring correlations between the thermal radiation and the later burst of negative energy, $I_{\text{lost}} = S_{\text{Bol}}$. This information cannot be recovered from the thermal radiation before the arrival of the negative-energy burst. After the burst of negative energy all the correlations between the particles and antiparticles are restored, and we get a pure state of zero entropy. This is expected since we impose reflecting boundary conditions and our spacetime has a trivial topology. Therefore, the information ΔI that is gained during the arrival of the burst of negative energy equals I_{lost} ,

$$\Delta I = I_{\text{lost}} = S_{\text{Bol}} \simeq \frac{N}{6} \ln \left(\frac{4M}{\lambda\kappa} \right) . \quad (65)$$

As we approach the critical solution, ΔI remains finite. Using (61) and (65) we get

$$\dot{I} = \frac{\Delta I}{\Delta u} \geq \frac{N\lambda}{48} \ln \left(\frac{4M}{\lambda\kappa} \right) \frac{\kappa}{(\lambda x_m^+)^2} \left(\frac{\partial x_B^+}{\partial x^-} \right)_{\text{max}} . \quad (66)$$

As the critical solution is approached, $\dot{I} \rightarrow \infty$.

Even though our space is one dimensional, the result (66) suggests that the way information is transferred by the negative-energy burst is different from that by which information is transferred in *linear* channels. The theoretical upper-bound on the bulk of information flow in N linear channels is [37]

$$\dot{I}_{\text{linear}} \leq \frac{E}{2\pi\hbar} \ln(N), \quad (67)$$

where the “message” is transferred with positive energy E . Suppose that this bound could be extended to negative energies, $E < 0$, by replacing E in (67) by $|E|$. From Eq. (63), we find

$$|E| \simeq \frac{\kappa\lambda}{4} \ln\left(\frac{4M}{\kappa\lambda}\right). \quad (68)$$

Then the theoretical upper bound (67) for our system would be

$$\dot{I}_{\text{linear}} \leq \frac{N\lambda}{96\pi} \ln\left(\frac{4M}{\kappa\lambda}\right) \ln(N). \quad (69)$$

For any given sufficiently large value of N one can find a range of solutions just below criticality for which the semiclassical approximation remains valid (i.e., the fluctuations (57) are small) while the bound (69) on \dot{I}_{linear} is exceeded by \dot{I} in (66). This is achieved by requiring that $\sqrt{N} \gg (\partial v_B / \partial u)_{\text{max}} > \ln(N) / 8\pi$.

It may be better to view the information associated with the negative energy in terms of information storage rather than information transfer. The brief burst of negative energy can be considered as a very localized configuration containing a finite amount of information that is traveling in space. As one approaches criticality the density of stored information becomes unbounded. This seems to be in agreement with other considerations regarding the unboundedness of information storage densities in quantum systems [38].

VII. CONCLUSIONS

In this work we present and study in detail a theory of semiclassical 2D dilaton gravity with reflecting (conformal) boundary conditions. This theory shares many of the features of spherically symmetric semiclassical gravity. In particular, massless scalar fields can collapse to form a black hole that evaporates. If the energy and energy density of the initial configuration of the scalar fields are below certain critical values, i.e., the subcritical or weak initial data case, then the scalar fields do not form a black hole, but instead are reflected from the boundary and escape to infinity. On the other hand, if the energy and energy density are above the critical values, i.e., the supercritical or strong initial data case, then the scalar fields collapse to form a black hole. This created black hole evaporates by emitting Hawking radiation. In a previous work [10] we found that such evaporation leads to an end-state geometry similar to that of a 4D semi-infinite throat. Here we study subcritical solutions, especially those near criticality, for general smooth initial data.

By combining analytical and numerical techniques we investigate the detailed structure of the classical and quantum one-loop contributions to the outgoing radiation reaching asymptotic future null infinity, \mathfrak{S}_R^+ . For the subcritical solutions, we find that before the reflected massless classical matter fields reach \mathfrak{S}_R^+ , positive-energy quantum radiation is observed at \mathfrak{S}_R^+ and continues as the classical matter reaches \mathfrak{S}_R^+ . This positive-energy quantum radiation is followed by a flux of negative-energy quantum radiation.

For profiles of incoming classical matter that encode information in bits consisting of pulses of two different amplitudes, we calculate how the encoded information appears in the outgoing classical profile on \mathfrak{S}_R^+ . For the quantum radiation, the situation is more involved. The outgoing positive-energy quantum radiation by itself does not describe a pure state, but is strongly correlated with the negative-energy quantum radiation reaching \mathfrak{S}_R^+ at a later time. This negative-energy quantum radiation not only insures conservation of energy but also restores the correlations necessary for a pure final quantum state.

The study of solutions just below and at criticality gives insight into the information puzzle in a unitary framework. As one approaches the critical solution the classical outgoing radiation becomes very distorted at late times. Part of that classical radiation reaches \mathfrak{S}_R^+ with a time-delay and has the form of an extremely dense brief pulse. As the critical solution is approached the late-time classical energy density becomes highly distorted and ultimately diverges, making it impossible to recover the complete classical information. Regarding the quantum radiation, as one approaches the critical solution the early-time radiation is indistinguishable from thermal Hawking radiation from a black hole, while the energy density of the late-time negative-energy radiation diverges, making recovery of the quantum correlations impossible. Although the late-time energy density of the outgoing radiation is infinite in the critical case, the total amount of energy is finite and conserved. Nevertheless, the semiclassical approximation breaks down because the fluctuations in $\hat{T}_{\mu\nu}^f$ become very large.

The above analysis shows that the black hole phase transition (subcritical \rightarrow supercritical) and the information puzzle are intimately related. At the critical solution there is an apparent breakdown of predictability. However, this breakdown of predictability is related to the breakdown of the semiclassical approximation. The same divergence in energy density that makes recovery of information and quantum correlations impossible evidently makes the semiclassical approximation invalid due to large fluctuations in $\hat{T}_{\mu\nu}^f$. We would like to stress that even though we take the large N limit to enforce the validity of the semiclassical approximation for subcritical solutions, the semiclassical approximation nevertheless breaks down at criticality. This may suggest that the breakdown of the semiclassical approximation at the onset of black hole formation is a fundamental result independent of the specific model to be studied. This is supported by the fact that the crucial features discussed in Sec. V B, i.e., the finite redshift factor and infinite blueshift factor, seem to be independent of the explicit semiclassical model. Thus, based on the semiclassical approximation alone, it may not be possible to trace the fate of information and correlations at the onset of black hole formation. The full quantum theory appears crucial to understanding if the overall evolution can be unitary at and after the onset of black hole formation. Nevertheless, our results do show that as criticality is approached via subcritical solutions, information and correlations become essentially irrecoverable while unitary evolution is preserved.

Acknowledgments

We thank B. Allen, L. Ford, J. Friedman, and T. Roman for helpful discussions, and R. Landauer for bringing to our attention the unboundedness of information storage densities in quantum systems. This work was supported by the National Science Foundation under Grant No. PHY 95-07740.

REFERENCES

- [1] S.W. Hawking, *Comm. Math. Phys.* **43**, 199 (1975).
- [2] J. Bekenstein, *Phys. Rev. D* **7**, 2333 (1973).
- [3] S.W. Hawking, *Phys. Rev. D* **14**, 2460 (1976).
- [4] G. 't Hooft, *Nucl. Phys. B* **256**, 727 (1985); **335**, 138 (1990).
 C.R. Stephens, G. 't Hooft and B.F. Whiting, *Class. Quantum Grav.* **11**, 621 (1994).
 Y. Aharonov, A. Casher, and S. Nussinov, *Phys. Lett. B* **191**, 51 (1987).
 L. Susskind, *Phys. Rev. Lett.* **71**, 2367 (1993); L. Susskind, L. Thorlacius, and J. Uglum,
Phys. Rev. D **48**, 3743 (1993).
 J. Bekenstein, *Phys. Rev. Lett.* **70**, 3680 (1993).
- [5] N.D. Birrell and P.C.W. Davies, *Quantum Fields in Curved Space*, (Cambridge University Press, Cambridge, England, 1982).
- [6] J. Harvey and A. Strominger, in *Recent Directions in Particle Theory: From Superstrings and Black Holes to the Standard Model (TASI-92)*, Proceedings of the Theoretical Advanced Summer Institute, Boulder, Colorado, edited by J. Harvey and J. Polchinski (World Scientific, Singapore, 1993);
 A. Strominger, “Les Houches Lectures Black Holes”, in *Les Houches Summer School, Session 62: Fluctuating geometries in Statistical Mechanics and Field theory*, Les Houches, France, 1994.
 T. Banks, “Lectures on Black Holes and Information Loss”, Spring school on Supersymmetry, Supergravity and Superstrings, Trieste, hep-th/9412131 (1994).
 S. Giddings, “Quantum Mechanics of Black Holes”, Summer School in High Energy Physics and Cosmology, Trieste, hep-th/9412138 (1994).
- [7] S.P. deAlwis, *Phys. Lett. B* **289**, 278 (1992); **300**, 330 (1993);
- [8] A. Bilal and C. Callan, *Nucl. Phys. B* **394**, 73 (1993).
- [9] J. Russo, L. Susskind and L. Thorlacius, *Phys. Rev. D* **46**, 3444 (1992).
- [10] S. Bose, L. Parker and Y. Peleg, *Phys. Rev. D* **52**, 3512 (1995).
- [11] J. Cruz and J. Navarro-Salas, “Solvable models of radiating Black Holes and Area-preserving Diffeomorphism”, Valencia Univ. report No. FTUV-95-31, hep-th@xxx/9512187 (1995).
 J. Cruz, J. Navarro-Salas, M. Navarro, and C.F. Talavera, “Symmetries and Black Holes in 2D Dilaton Gravity”, Valencia Univ. report, hep-th@xxx/9606097 (1996).
- [12] T. Chung and H. Verlinde, *Nucl. Phys. B* **418**, 305 (1994).
- [13] A. Strominger and L. Thorlacius, *Phys. Rev. D* **50**, 5177 (1994).
- [14] S.R. Das and S. Mukherji, *Mod. Phys. Lett. A* **9**, 3105 (1994).
- [15] S. Bose, L. Parker and Y. Peleg, *Phys. Rev. Lett.* **76**, 861 (1996).
- [16] M.W. Choptuik, *Phys. Rev. Lett.* **70**, 9 (1993).
 A.M. Abrahams and C.R. Evans, *Phys. Rev. Lett.* **70**, 2980 (1993).
 J. Coleman and C.R. Evans, *Phys. Rev. Lett.* **72** 1842 (1994).
 P.R. Brady, *Class. Quant. Grav.* **11**, 1255 (1994); *Phys. rev. D* **50**, 7144 (1994).
 Y. Oshiro, K. Nakamura and A. Tomimatso, *Prog. Thoer. Phys.* **91**, 12665 (1994).
 J. Traschen, *Phys. Rev. D* **50**, 7144 (1994).
 V. Husain, E. Martinez and D. Nunez, *Phys. Rev. D* **50**, 3783 (1994) .
 Y. Peleg and A.R. Steif, *Phys. Rev. D* **51**, 4198 (1995).

- D.M. Eardley, E.W. Hirschman and J. Horne, Phys. Rev. D **52**, 5397 (1995).
 C. Gundlach, R.H. Price, and J. Pullin, Phys. Rev. D **49**, 890 (1994).
 D. Garfinkle, Phys. Rev. D **51**, 5558 (1995).
- [17] G.W. Gibbons and K. Maeda, Nucl. Phys. B **298** 741 (1988);
 D. Garfinkle, G. Horowitz and A. Strominger, Phys. Rev. D **43**, 3140 (1991).
- [18] Y. Peleg, Mod. Phys. Lett. A **9**, 3137 (1994).
- [19] C. Callan, S. Giddings, J. Harvey and A. Strominger, Phys. Rev. D **45**, 1005 (1992).
- [20] A. Polyakov, Phys. Lett. B **103**, 207 (1981).
- [21] T.M. Fiola, J. Preskill, A. Strominger and S.P. Trivedi, Phys. Rev. D **50**, 3987 (1994).
- [22] A. Miković, Class. Quant. Grav. **13**, 209 (1996); Phys. Lett. B **291**, 19 (1992); B **304**, 70 (1993).
- [23] S. Deser, M.J. Duff and C.J. Isham, Nucl. Phys. B **111**, 45 (1976).
- [24] P.C.W. Davies S.A. Fulling and W.G. Unruh, Phys. Rev. D **13**, 2720 (1976).
 P.C.W. Davies, Proc. R. Soc. London, A **354**, 529 (1976).
- [25] S.A. Fulling and P.C.W. Davies, Proc. R. Soc. London, A **348**, 393 (1976).
- [26] J. Russo, L. Susskind and L. Thorlacius, Phys. Lett. B **292**, 13 (1992).
- [27] W.H. Press, S.A. Teukolsky, W.T. Vetterling and B.P. Flanney, *Numerical Recipes in C*, (Cambridge Univ. Press, Cambridge, 1992).
- [28] A. Bilal and I.I. Kogan, Phys. Rev. D **47**, 5408 (1993).
- [29] S. Bose, L. Parker and Y. Peleg, Phys. Rev. D **53**, 7089 (1996).
- [30] D. Christodoulou, Commun. Math. Phys. **105**, 337 (1986).
- [31] L.H. Ford and T.A. Roman, Phys. Rev. D **53**, 1988 (1996).
- [32] R.B. Carlitz and R.S. Willey, Phys. Rev. D **36**, 2327; 2336 (1987).
 F. Wilczek, Princeton-IAS Report No. IASSMS-HEP-93-12, hep-th/9302096, (1993).
- [33] C. Kuo and L.H. Ford, Phys. Rev. D **47**, 4510 (1994).
- [34] A. Miković and V. Radovanović, “Two-loop Beack-reaction in 2D Dilaton Gravity”,
 Chalmers Univ. report no. Goteburg-ITP-96-7, hep-th@xxx/9606098 (1996).
- [35] L. Parker, Phys. Rev. D **12**, 1519 (1975).
 R.M. Wald, Commun. Math. Phys. **45**, 9 (1975).
- [36] S.B. Giddings and W. M. Nelson, Phys. Rev. D **46**, 2486 (1992).
- [37] L.B. Levitin, Int. J. Theor. Phys. **21**, 299 (1982);
 J.D. Bekenstein and M. Schiffer, Int. J. Mod. Phys. C **1**, 355 (1990);
 H.J. Bremermann, Int. J. Theor. Phys. **21** 203 (1982).
 See also R. Landauer in Ref. [38] .
- [38] R. Landauer, “Information is Physical”, in *Proceedings of the Workshop on Physics and Computation*, PhysComp '92, October 2-4 1992, Dallas, Texas; “Minimal energy requirements in communication”, IBM report (1995).

FIGURES

FIG. 1. Penrose diagram of the Linear Dilaton solution. The heavy curve is the boundary curve separating the regions of weak and strong coupling.

FIG. 2. Penrose diagram of a typical subcritical solution. The infalling matter with support on the interval $x_1^+ < x^+ < x_2^+$ on \mathfrak{S}_R^- , is reflected from the boundary to become outgoing toward future null infinity, \mathfrak{S}_R^+ . Here $z = \lambda x^-$.

FIG. 3. The incoming stress tensor, $T_{vv}(v)$, for three different families of initial data, with (a) corresponding to Eq. (32), (b) corresponding to Eq. (38) and (c) corresponding to Eq. (40).

FIG. 4. The stress tensor T_{uu} in units of λ^2 describing the outgoing radiation on \mathfrak{S}_R^+ . The solid curves describe the total outgoing radiation, T_{uu}^f , while the gray curves describe only the quantum part, $\langle T_{uu} \rangle$, scaled by $2/\kappa$. In (a) the mass is about 6% and in (b) it is about 65% of the critical mass for the infalling matter shown in Fig. 3(a). In (c) the mass is about 3% and in (d) it is about 65% of the critical mass for the case shown in Fig. 3(b).

FIG. 5. The stress tensor T_{uu} describing the outgoing radiation for different values of $\lambda\epsilon$ in the case of the infalling matter shown in Fig. 3(a) with $M/\lambda = 0.1$. See the text for more details.

FIG. 6. The stress tensor T_{uu} describing the outgoing radiation for the infalling matter shown in Fig. 3(c). The solid curves describe the total outgoing radiation, while the gray curves describe only the quantum part. In (a) the mass is about 4% of the critical mass, while in (b) it is about 80% of the critical mass.

FIG. 7. The relative correlation function of the outgoing quantum radiation on \mathfrak{S}_R^+ . In (a) the mass is about 6% of the critical mass, while in (b) it is 99.999% of the critical mass.

FIG. 8. The stress tensor T_{uu} describing the outgoing radiation for nearly critical solutions with M being 99.999% of the critical mass. In (a) we plot the total outgoing radiation and in (b) only the quantum part is plotted. The dashed, dotted and gray curves correspond to the infalling matter shown in Figs. 3(a), 3(b) and 3(c), respectively.

FIGURE 1

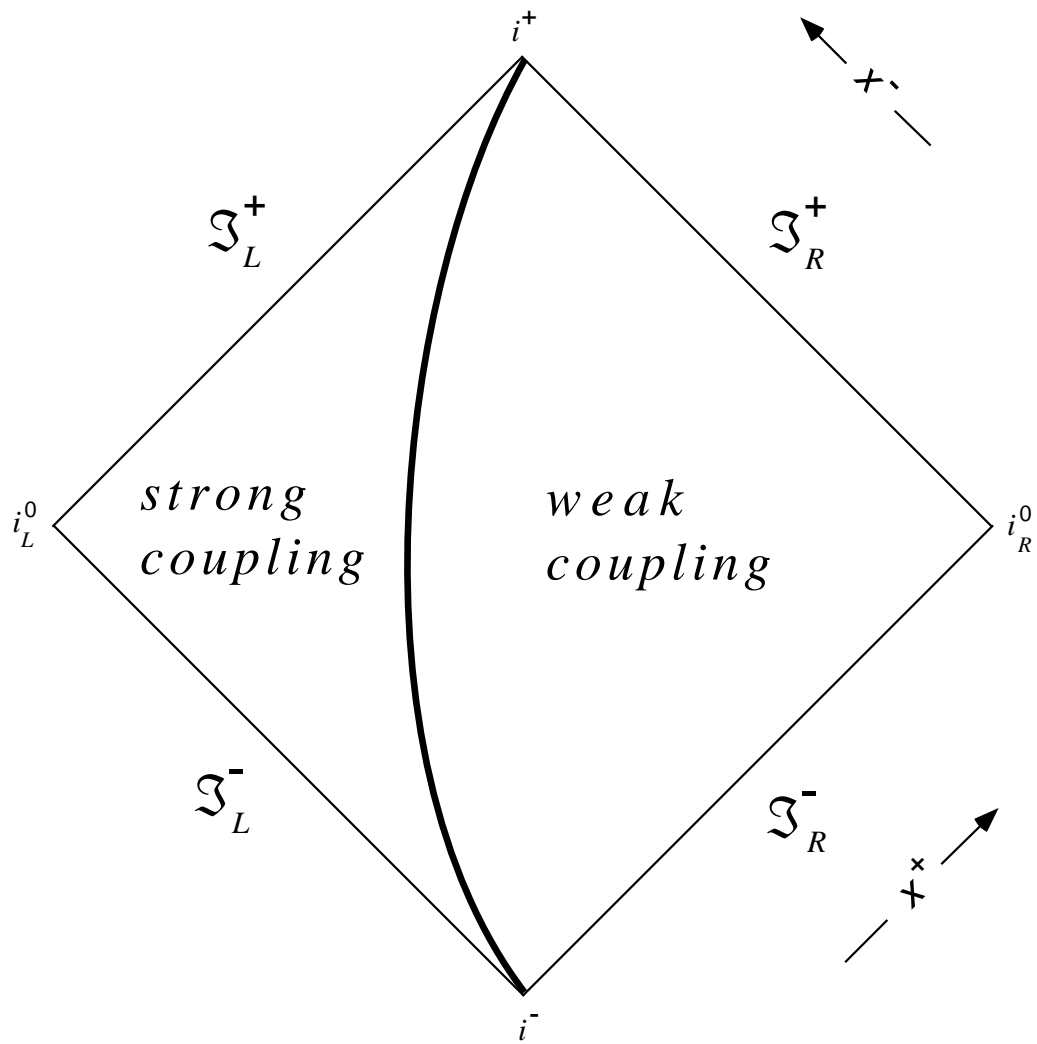


Fig. 1: Penrose diagram of the Linear Dilaton solution. The heavy curve is the boundary curve separating the regions of weak and strong coupling.

FIGURE 2

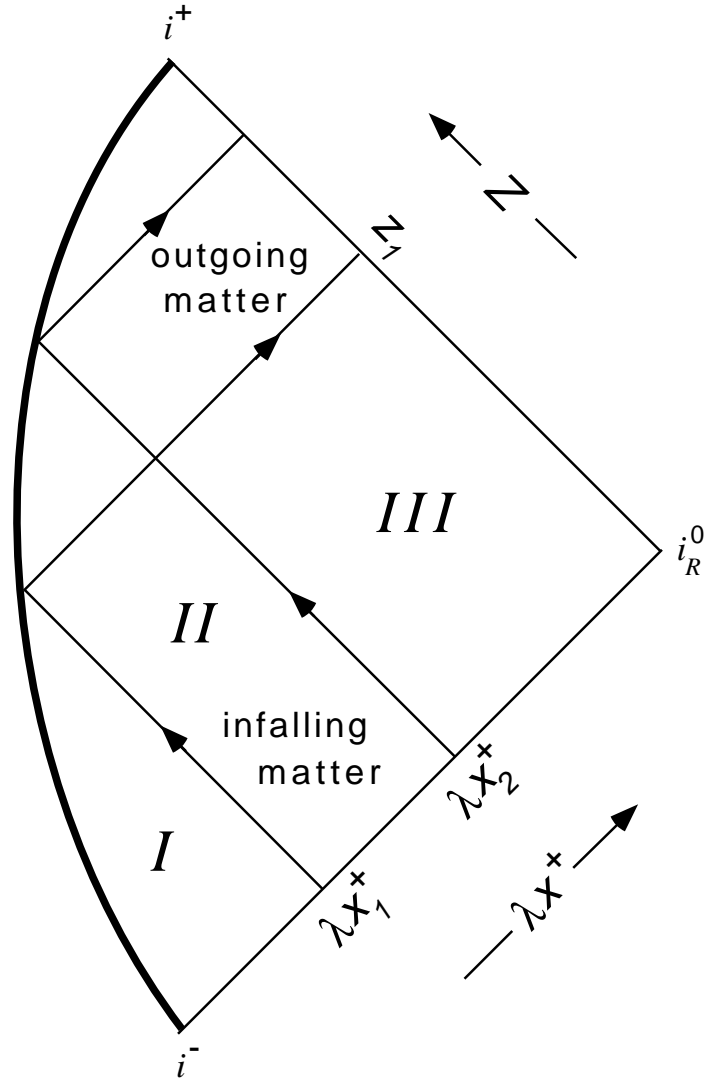


Fig. 2: Penrose diagram of a typical subcritical solution. The infalling matter with support on the interval $x_1^+ < x^+ < x_2^+$ on \mathfrak{S}_R^- , is reflected from the boundary to become outgoing toward future null infinity, \mathfrak{S}_R^+ . Here $z = \lambda x^-$.

FIGURE 3

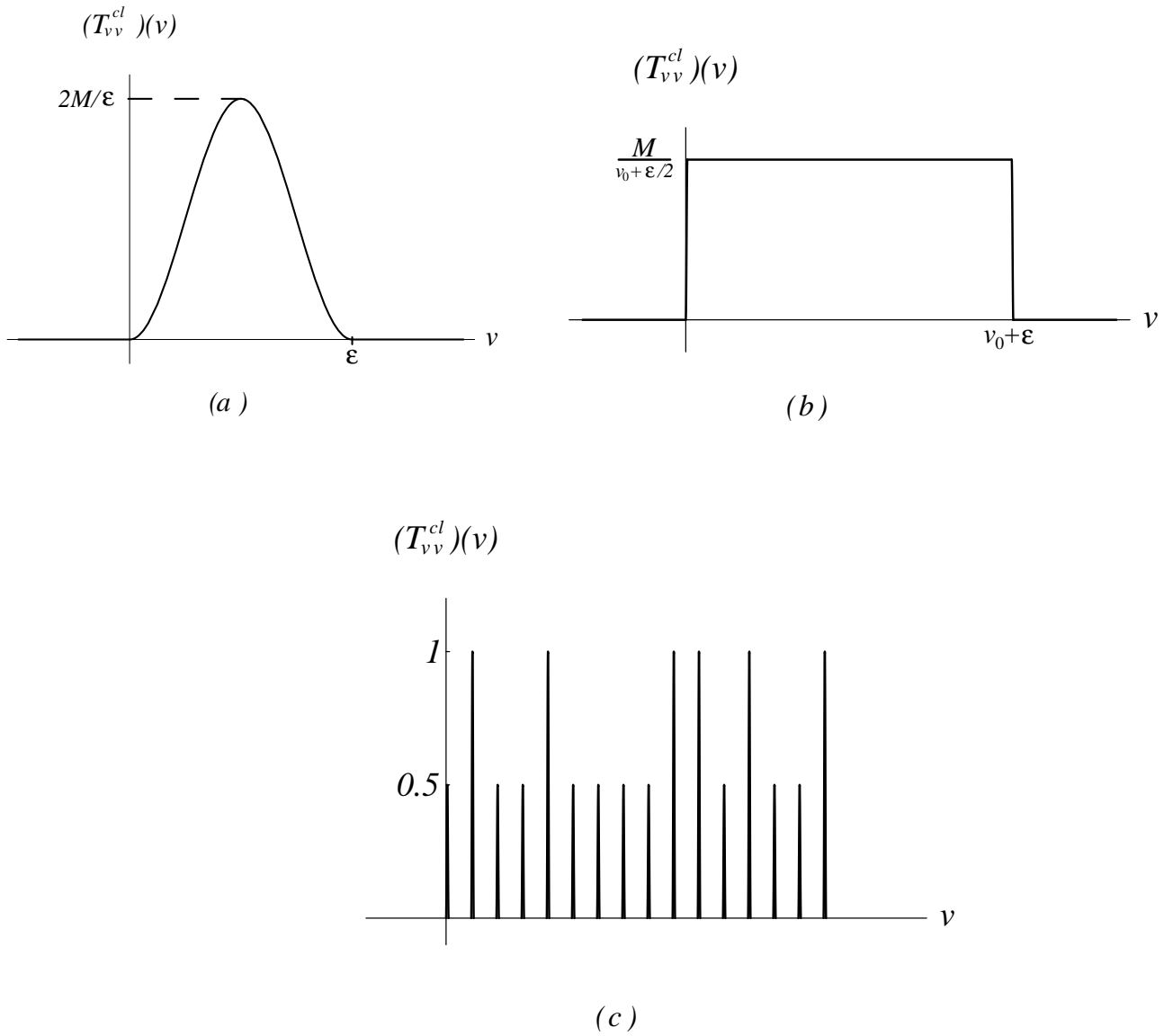


Fig. 3: The incoming stress tensor, T_{vv} , for three different families of initial data, with (a) corresponding to Eq. (32), (b) corresponding to Eq. (38), and (c) corresponding to Eq. (40).

FIGURE 4

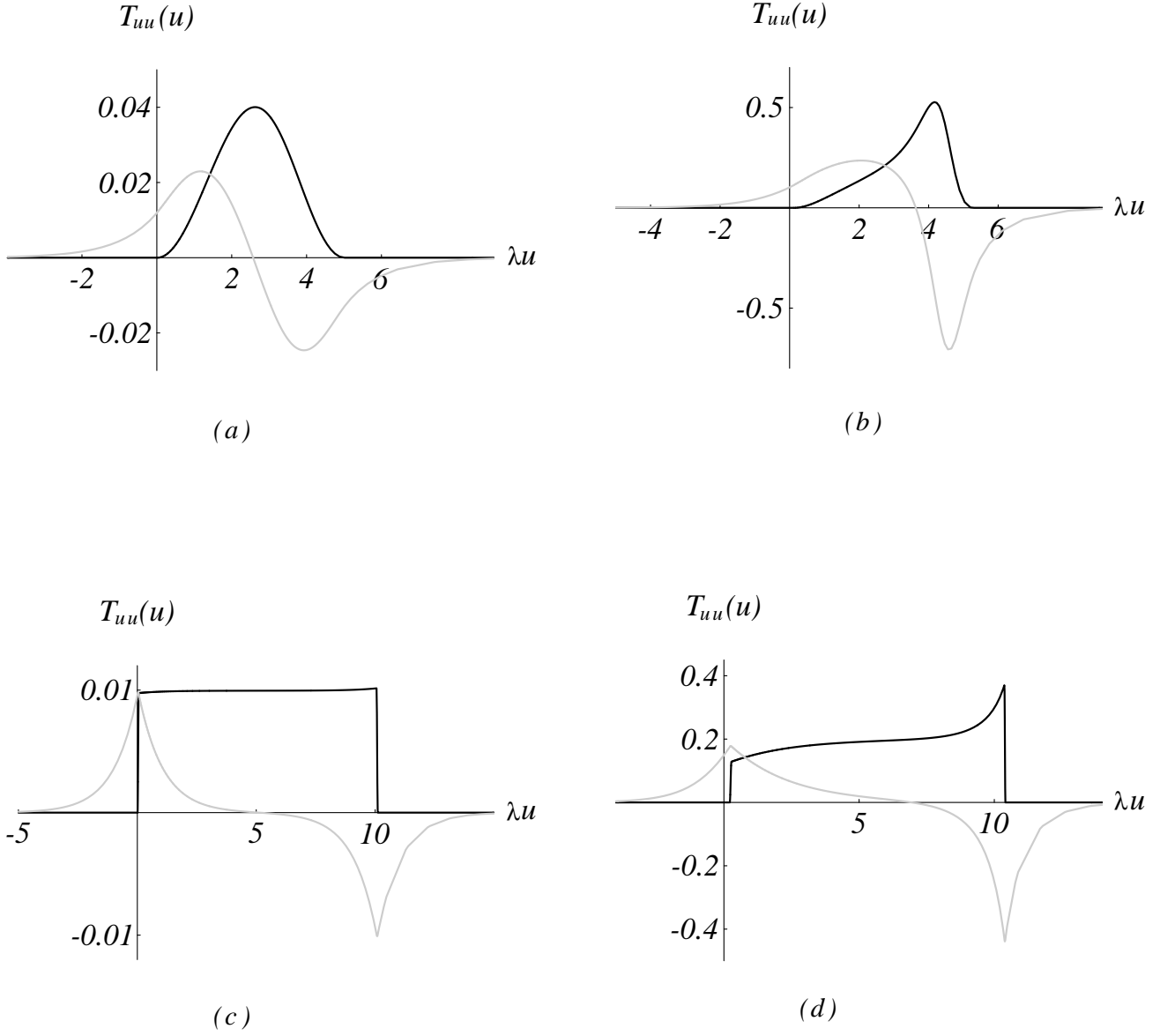


Fig. 4: The stress tensor, T_{uu} in units of λ^2 describing the outgoing radiation on \mathfrak{S}_R^+ . The solid curves describe the total outgoing radiation, T_{uu}^f , while the gray curves describe only the quantum part, $\langle T_{uu} \rangle$, scaled by $2/\kappa$. In (a) the mass is about 6% and in (b) it is about 65% of the critical mass for the infalling matter shown in Fig. 3(a). In (c) the mass is about 3% and in (d) it is about 65% of the critical mass for the case shown in Fig. 3(b).

FIGURE 5

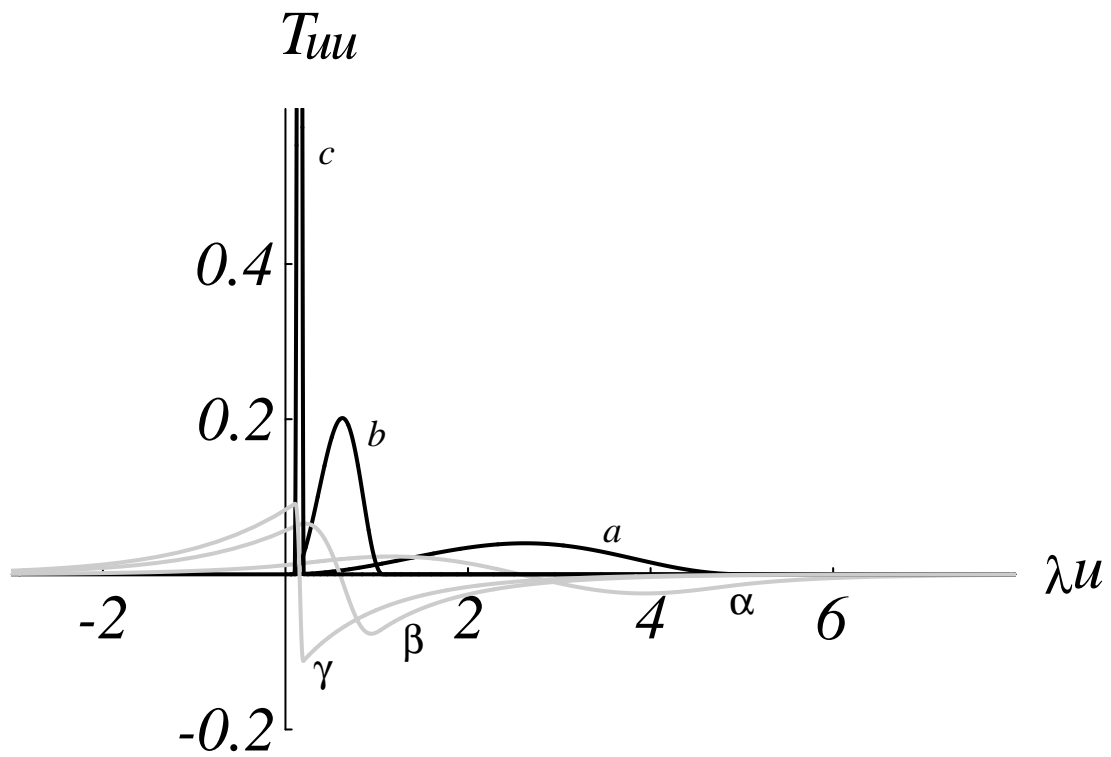


Fig. 5: The stress tensor T_{uu} describing the outgoing radiation for different values of $\lambda\epsilon$ in the case of the infalling matter shown in Fig. 3(a) with $M/\lambda = 0.1$. See the text for more details.

FIGURE 6

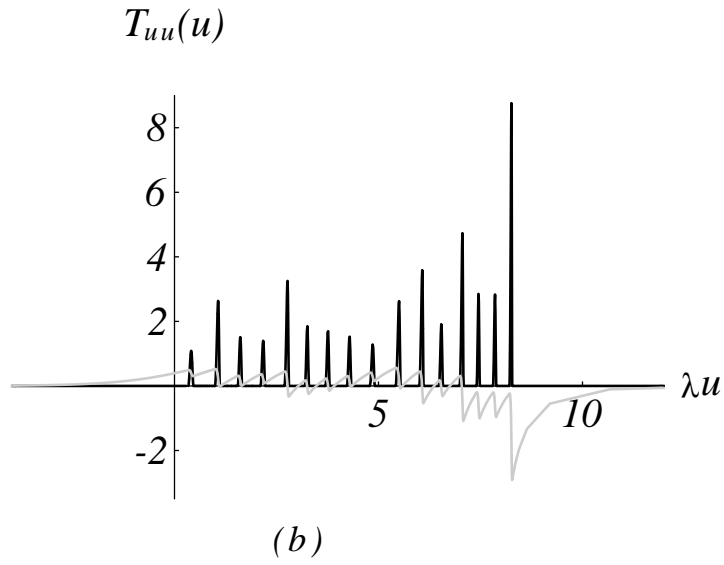
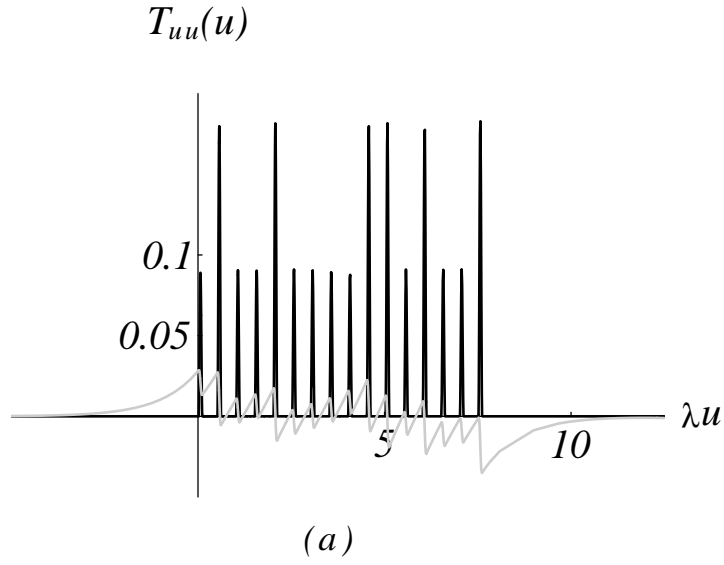
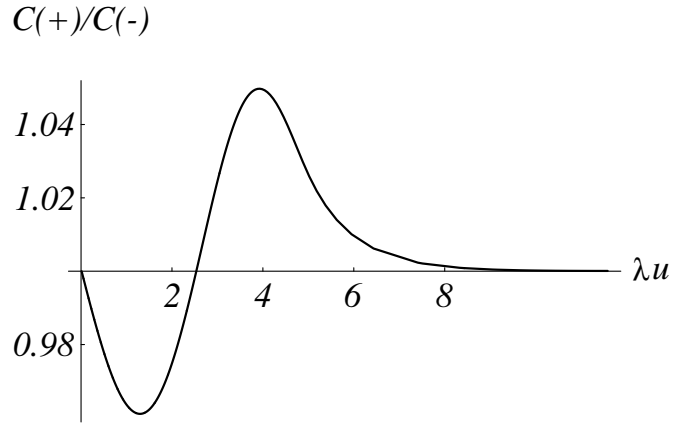
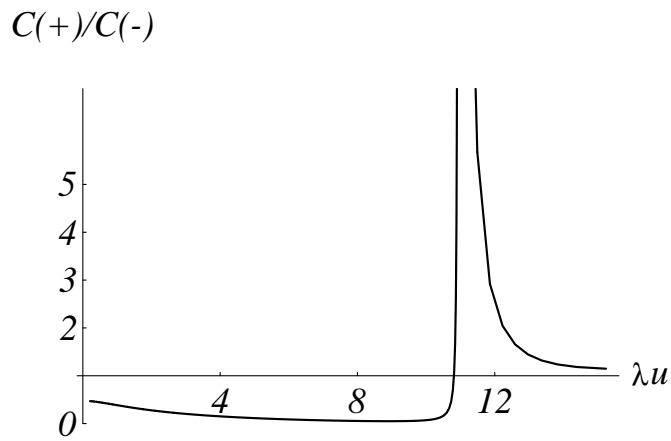


Fig. 6: The stress tensor T_{uu} describing the outgoing radiation for the infalling matter shown in Fig. 3(c). The solid curves describe the total outgoing radiation, while the gray curves describe only the quantum part. In (a) the mass is about 4% of the critical mass, while in (b) it is about 80% of the critical mass.

FIGURE 7



(a)



(b)

Fig. 7: The relative correlation function of the outgoing radiation on \mathfrak{S}_R^+ . In (a) the mass is about 6% of the critical mass and in (b) it is 99.999% of the critical mass.

FIGURE 8

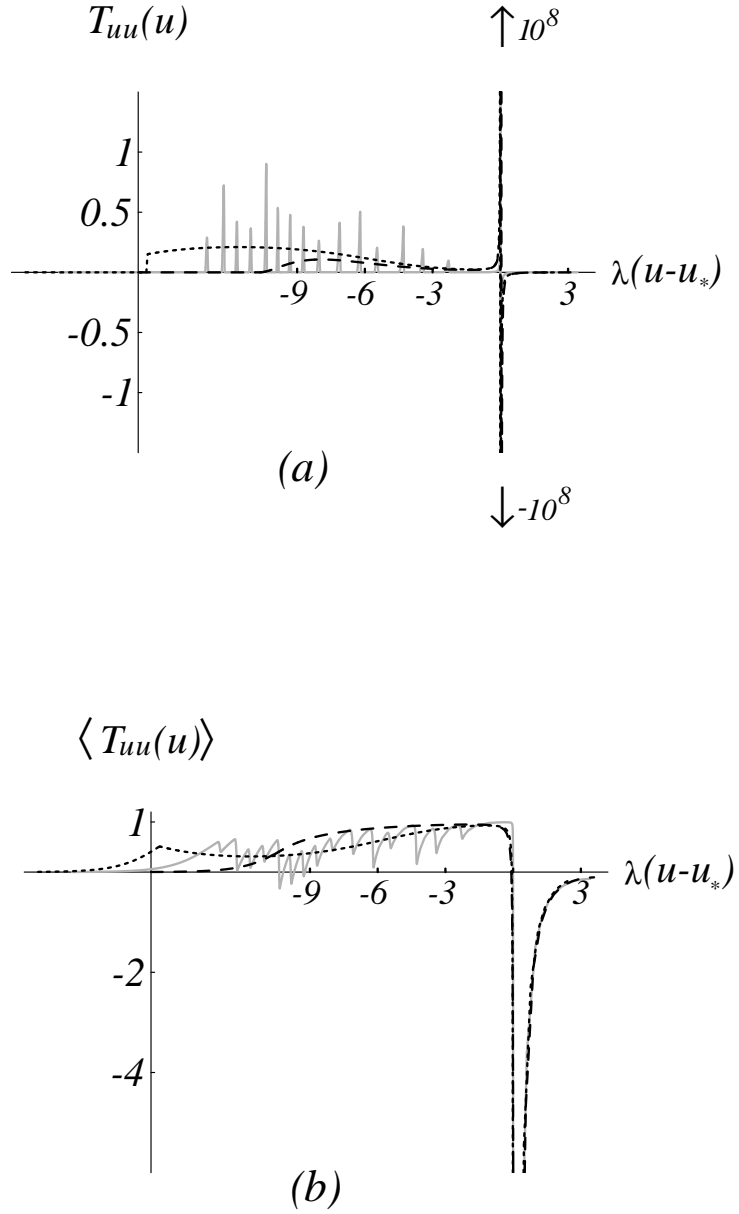


Fig. 8: The stress tensor T_{uu} with M being 99.999% of the critical mass. In (a) we plot the total outgoing radiation and in (b) only the quantum part is plotted. The dashed, dotted and gray curves correspond to the infalling matter shown in Figs. 3(a), 3(b), and 3(c) respectively.